Cellular Damage by Auger Electrons from ^{123}I

Moruri Letty Dimpho

A dissertation submitted in partial fulfillment of the requirements for the degree of Master of Science in Applied Radiation Science and Technology (ARST) in the faculty of Agriculture, Science and Technology at the North West University.

060001797U

North-West University
Mafikeng Campus Library

Supervisor : Dr J. P. Slabbert

Radiation Biophysics

iThemba LABS

b16914247
B18699029

B714.876

February 2005

LIBRARY
MAFIKENG CAMPUS
Call No.: TH 571.6345
2006 -02- 15 mor
Acc. No.: 06/A0328
NORTH-WEST UNIVERSITY

ABSTRACT

Auger electrons have the potential for therapy mainly because of their short range and high level of toxicity. Biological effects of these electrons are critically dependent on the cellular and sub-cellular localization of their emitters. In this study, ^{123}I was used due to its relatively short half-life (13.2 h) and ideal γ-ray energy (E_γ=159 keV). The short half-life is advantageous since it allows significant accumulation of disintegrations at normal physiological conditions without the need to freeze cells as required when long lived isotopes such as ^{125}I ($T_{1/2}$=60.1 days) are used. The main objective of this study was to synthesize an organic compound that would deliver the radioactive ^{123}I into cellular DNA and to quantify the resulting damage from micronucleation.

The higher degree of damage obtained in cell samples treated with 4-[^{123}I]iodoantipyrine than with [^{123}I]NaI is an indication of Auger electron effect. Also, micronuclei counts showed that 4-[^{123}I]iodoantipyrine and [^{123}I]NaI were prepared in a suitable manner and did not interfere with cellular kinetics. RBE values of 1.8 and 1.9 were obtained for CHO-K1 clone # 7 and # 16 cells, respectively, indicating lack of differential response for the two clones. When the current data is collectively analyzed with that of other investigators using the same radiolabeled compounds, a reduction in Auger electron RBE is noticeable with radiosensitivity. This is consistent with the high-LET nature of Auger electrons. The extremely radiosensitive CHO-XRS 1 failed to give a dose-response as most cells underwent apoptosis. The significant radioprotection of CHO-K1 cells irradiated, in the presence of a chemical protector MEA, with 4-[^{123}I]iodoantipyrine than with [^{123}I]NaI showed that the mode by which Auger electrons cause damage is not the same as that of α-particles. Further studies involving the use of carriers that would specifically deliver radionuclides to nuclear DNA may be useful in understanding the mechanisms underlying the cellular responses to Auger electron exposure.

250297745

DECLARATION

I hereby declare that the work contained in this dissertation is my own work and has not been submitted for any degree or any other qualification in any other university or institution.

Signed ..... Date 31/03/2005

Moruri Letty Dimpho

ACKNOWLEDGEMENTS

I will like to thank, first and foremost my supervisor - Dr Slabbert for his fatherly, professional and structural supervision. His guidance, persistence and great expertise in the field has been worthwhile towards the success of this dissertation. North West university and iThemba LABS for introducing me to this adventurous and exciting world of nuclear technology. A 'special thank you' goes to Mr. Stuart Dolley for his invaluable patience in organic compound synthesis and radiolabeling experiments. Without him, this work would have never seen the light of day.

Mr. Timothy Sebeela for his assistance with cell culture experiments throughout this study. Your contribution never went unnoticed.

Dr John Akudugu, for his last minute input which made writing this thesis much easier. His constructive criticism, sympathetic ear whenever I approached him for advice and not forgetting that warm smile of welcome.

My parents - Mr. and Mrs. Moruri - Ke lebogela kgodiso le thotloetso ya lona. I am who I am because of the love and sacrifices you made for me. You are by idols.

Last but not least, God the Almighty for granting me the courage, guidance and serenity to tackle such a challenging and demanding task.

TABLE OF CONTENTS

Abstract		i
Declaration		ii
Acknowledgements		iii
Table of contents		iv
List of abbreviations		viii
List of figures		ix
List of tables		xiii

Chapter 1 : Introduction to the study and research problem

1.1	Introduction	1
1.2	Choosing the best radionuclide for therapy	2
1.3	Choosing the isotope delivery agent	3
1.4	Motivation for doing the study	4
1.5	Purpose of the study	6

Chapter 2 : Literature Review 8

2.1	History of Auger electrons	8
2.2	Biological significance of Auger electrons	9
2.3	LET and RBE relationship	10
2.4	Radionuclides for medical use	12

2.5 Diagnostic radionuclides used in targeted therapy 14

2.6 β-emitters as a source of radiation for targeted therapy 15

2.7 α-emitters as source of radiation for targeted therapy 17

2.8 Auger electrons as source of radiation for targeted therapy 18

2.9 Cellular effects of Auger electrons in biological cells 18

2.10 The indirect effect of Auger in causing biological damage 19

2.5.2 The use of radioprotectors in Auger electron radiation 20

Chapter 3 : Research Materials and Methods 23

3.1 Production of ^{123}I 23

3.2 Synthesis of delivery agent 4-iodoantipyrine 26

3.3 Chromatogram analysis 27

3.4 Radioactive labeling by ion exchange 29

3.4.1 Preparation of 0.1 mg 4-iodoantipyrine reaction vials 29

3.4.2 Reaction mixture 30

3.4.3 Purification column 30

3.5 Preparation of labeled 4-[^{123}I]iodoantipyrine and unlabeled [^{123}I]NaI for cell irradiations 33

3.6 Radioactivity measurements for labeled and unlabeled compounds 33

3.7 Cell types, storage and culture maintenance 34

3.7.1 Cell types 34

3.7.2 CHO cell storage and culture maintenance 35

3.8 Preparation of CHO-K1 #16 for irradiation with ^{60}Co γ-rays and micronucei analysis 36

3.9 Irradiation of CHO cells with 4-[^{123}I]iodoantipyrine and [^{123}I]NaI 37

3.10 Irradiation of CHO cells in the presence of β-mercaptoethylamine (MEA) 37

3.11 Identification and counting of micronuclei 38

3.12 Isolation of T-lymphocytes from a whole blood sample 39

3.12.1 Lymphocytes irradiation and culturing 40

3.12.2 Lymphocyte cell fixing and slide preparation for micronuclei counting 41

3.13 Radiation dosimetry 41

Chapter IV : RESULTS AND DISCUSSIONS 43

4.1 Ion exchange results 43

4.1.1 Run #1: first radiolabeling 43

4.1.2 Run #2: second radiolabeling 46

4.1.3 Run #3: third radiolabeling 48

4.1.4 Run #4: fourth radiolabeling 50

4.1.5 Run #5: fifth radiolabeling 52

4.1.6 Summary of labeling results 53

4.2 Results of cellular irradiation 54

4.2.1 Irradiation of CHO-K1 cells in frozen state and room temperature 54

4.3 Irradiation of CHO-K1 #16 cells with 4-[^{123}I]iodoantipyrine and [^{123}I]NaI 58

4.4 Irradiation of T-lymphocytes with 4-[^{123}I]iodoantipyrine and [^{123}I]NaI 64

4.5 Irradiation of T-lymphocytes with 4-[^{123}I]iodoantipyrine and [^{123}I]NaI in the presence of a radioprotector β-mercaptoethylamine (MEA) 68

4.6 Irradiation of CHO-K1 clone #16 cells with 4-[^{123}I]iodoantipyrine and [^{123}I]NaI in the presence of a radioprotector β-mercaptoethylamine (MEA) 71

4.7 Radiosensitivity tests using ^{60}Co γ-rays 75

4.8 Irradiations of CHO-XRS 1 cells with 4-[^{123}I]iodoantipyrine and [^{123}I]NaI 76

4.9 Irradiation of CHO-K1 clone #7 cells using 4-[^{123}I]iodoantipyrine and [^{123}I]NaI 79

4.10 Summary of irradiation results 83

Chapter 5 : Conclusions and Recommendations 86

5.1 Conclusions 86

5.2 Recommendations 88

LIST OF ABBREVIATIONS

µl	:	microliter
µm	:	micrometer
α-MEM	:	Alpha minimum essential medium
4-[^{123}I]IAP	:	4-[^{123}I]iodoantipyrine
BN	:	Binucleation
CHO-K1	:	Chinese hamster ovary cells K1
DMSO	:	Dimethylsulfoxide
FBS	:	Fecal Bovine Serum
Gy	:	Gray (S.I unit for radiation dose)
HPLC	:	High performance liquid chromatography
keV	:	kilo electron volts
LET	:	Linear energy transfer
MeV	:	Mega electron volts
ml	:	milliliter
MN	:	Micronuclei
NaI	:	Sodium iodide
PBS	:	Phosphate buffered solution
RBE	:	Relative biological effectiveness
rpm	:	revolutions per minute
RPMI 1640	:	Roswell Park Memorial Institute 1640

LIST OF FIGURES

Figure 2.1 Auger electron emissions.

Figure 2.2 The indirect and direct actions of ionizing radiation in the nuclear DNA. The letters S, T, P, A, G and C represent sugar, thiamine, phosphorus, adenine, guanine and cytosine, respectively .

Figure 3.1 The decay of parent nuclide (^{123}Xe) and growth of daughter nuclide (^{123}I) as a function of time.

Figure 3.2 The percentage decay of ^{123}Xe with respect to time.

Figure 3.3 A schematic diagram representing the chemical reaction between Antipyrine and NaI to produce 4-iodoantipyrine and the radiolabeling with ^{123}I to produce 4-[^{123I}]iodoantipyrine.

Figure 3.4 HPLC electronics.

Figure 3.5 A chromatogram showing 100% 4-iodoantipyrine (peak 1) after repeated crystallization.

Figure 3.6 Purification column and 4 elusion fractions.

Figure 3.7 Activity Counter.

Figure 3.8 A slide of CHO cells showing a mononucleated cell (A), a binucleated cell with no micronucleus (B), one micronucleus (C) and four micronuclei (D) after a 16-hour exposure to 4-[^{123}I]iodoantipyrine (1.2 dist/μm^3).

Figure 4.1 The labeling efficiency of fraction 1 as determined by HPLC. Peak-1 shows unbound ^{123}I to be more than 5%. Peak-2 indicates impurities that can be removed by filtration. Peak-3 shows that less than 95% of the antipyrine is labeled with ^{123}I.

Figure 4.2 The labeling efficiency of fraction 3 as determined by HPLC. The single peak indicates that 100% of the antipyrine is labeled with ^{123}I.

Figure 4.3 The labeling efficiency of fraction 4 as determined by HPLC. Peak-1 shows that 1.1% of the radioactivity was unbound and peak-2 represents the 98.9% antipyrine labeled with ^{123}I.

Figure 4.4 The labeling efficiency of fraction 4 as determined by HPLC. Peak-1 shows unbound ^{123}I to be less than 1.1%. Peak-2 shows ^{123}I bound to antipyrine to be 98.9%.

Figure 4.5 Chromatograph of fraction 4 showing 98.5% of antipyrine bound ^{123}I (peak 4) and 0.068% unbound ^{123}I (peak 1). Peak 2 and 3 shows some impurities that can be removed by filtration.

Figure 4.6 Chromatograph of fraction 3 showing 96.5% of antipyrine bound ^{123}I (peak 3). Only 1.7% was free ^{123}I (peak 1). Peak 2 indicates the presence of impurities that could be removed by filtration.

Figure 4.7 Chromatograph of fraction 4 showing 98.5% of antipyrine bound ^{123}I(peak 3) and 0.068% unbound ^{123}I (peak 1). Peak 2 shows some impurities that could be removed by filtration.

Figure 4.8 Dose response curves representing micronuclei frequency per 500 binucleated CHO-K1 cells irradiated with ^{60}Co at room temperature and in a frozen state.

Figure 4.9 Percentage binucleation for CHO-K1 cells irradiated at different dose points at room temperature and in a frozen state.

Figure 4.10 Dose response curves representing the number of micronuclei per 500 binucleated CHO-K1 #7 cells as a function of dose after exposure to 4-[^{123}I]iodoantipyrine and [^{123}I]NaI.

Figure 4.11 Dose response curves representing the number of micronuclei per 500 binucleated lymphocytes as a function of dose after exposure to 4-[^{123}I]iodoantipyrine and [^{123}I]NaI.

Figure 4.12 Micronuclei frequencies and radioprotection observed in CHO-K1 cells irradiated with 4-[^{123}I]IAP and [^{123}I]NaI in the absence and presence of MEA.

Figure 4.13 Micronuclei frequency observed in CHO-K1 #7, CHO-K1 #16 and CHO-XRS 1 cells irradiated with 2 Gy of ^{60}Co γ-rays.

Figure 4.14 Micronuclei frequencies showing biological damage in CHO-XRS 1 cells irradiated with 4-[^{123}I]Iodoantipyrine and [^{123}I]NaI.

Figure 4.15 Dose response curves representing the relationship between micronuclei frequencies per 500 binucleated CHO-K1 #7 cells irradiated with 4-[^{123}I]IAP and [^{123}I]NaI and the number of disintegrations per unit volume.

Figure 4.16 The ratios of the slopes of micronuclei-dose response curves for 4-[^{123}I]IAP (B) and [^{123}I]NaI (A) exposure in eleven cells lines as a function of radiosensitivity expressed as micronuclei frequency/disintegration/μm^3 with [^{123}I]NaI exposures.

LIST OF TABLES

Table 2.1 Radionuclides suitable for diagnosis and/or therapy. E_{max} is the maximum particle energy and E_γ is the energy of the corresponding γ -component.

Table 4.1 Measured activities of 4-[^{123}I]iodoantipyrine for each fraction collected from the purification column.

Table 4.2 Radioactivities measured for the final 4-[^{123}I]iodoantipyrine and [^{123}I]NaI preparation.

Table 4.3 Activities measured in elusion fractions and labeling efficiency by HPLC analysis.

Table 4.4 Final activities of 4-[^{123}I]iodoantipyrine and [^{123}I]NaI after filtration.

Table 4.5 Activities measured in elusion fractions and labeling efficiency by HPLC analysis.

Table 4.6 Final activities of 4-[^{123}I]iodoantipyrine and [^{123}I]NaI after filtration.

Table 4.7 Activities measured in elusion fractions and labeling efficiency by HPLC analysis.

Table 4.8 Measured activities of 4-[^{123}I]iodoantipyrine and [^{123}I]NaI after filtration.

Table 4.9 Activities measured in elusion fractions and labeling efficiency by HPLC analysis

Table 4.10 Measured activities of 4-[^{123}I]iodoantipyrine and [^{123}I]NaI after addition of medium and filtration.

Table 4.11 Micronuclei frequency distribution in binucleated CHO-K1 cells irradiated in frozen state.

Table 4.12 Micronuclei frequency distributions in binucleated CHO-K1 cells irradiated at room temperature.

Table 4.13 Cumulative doses (disintegrations per μm^3) of 4-[^{123}I]iodoantipyrine and [^{123}I]NaI to CHO-K1 cells in suspension.

Table 4.14 Micronuclei yield and proliferation (% BN) observed in CHO-K1 binucleated cells treated with 4-[^{123}I]iodoantipyrine.

Table 4.15 Micronuclei yield and proliferation (% BN) observed in CHO-K1 binucleated cells irradiated with [^{123}I]NaI.

Table 4.16 Biological disintegrations of 4-[^{123}I]iodoantipyrine and [^{123}I]NaI in human T-lymphocytes.

Table 4.17 Micronuclei frequency distributions observed in binucleated human T-lymphocytes irradiated with 4-[^{123}I]iodoantipyrine.

Table 4.26 Micronuclei frequency distributions observed in CHO-XRS 1 cells irradiated with [^{123}I]NaI.

Table 4.27 Disintegrations of 4-[^{123}I] Iodoantipyrine and [^{123}I] NaI in 1ml CHO-K1 cell suspensions.

Table 4.28 Micronuclei frequency distributions observed in CHO-K1 cells irradiated with 4-[^{123}I]iodoantipyrine.

Table 4.29 Micronuclei frequency distributions observed in CHO-K1 cells irradiated with [^{123}I]NaI.

Table 4.30 The slopes of dose responses expressed as micronuclei frequency per 500 binucleated cells/disintegrations /μm^3 for 4-[^{123}I]IAP and [^{123}I]NaI in various cells lines. A and B are the slopes for [^{123}I]NaI and 4-[^{123}I]IAP treatments, respectively. r is the regression coefficient.

CHAPTER I

1. Introduction to the study and research problem

1.1 Introduction

Auger electrons have gained a reputable place in radiotherapy treatment as a method for targeted therapy. Targeted therapy is mainly aimed at the eradication of micrometastatic lesions whilst sparing normal cells. This is achieved by the characteristic low energy (<500 eV) and short range (<25 nm) of Auger electrons in cells. Due to their short range, these particles have unique properties for inducing biological damage that is highly dependent upon their cellular and sub-cellular distribution. These low energy electrons are mainly emitted by radionuclides that decay by internal conversion (IC) and/or electron capture (EC).

Since energy deposition takes place in less than 25 nm, the biological damage induced by Auger electrons has lethal effects as severe as alpha particles and both have been classified as radiation with high linear energy transfer (LET) (Goddu *et al.*, 1994). Thus the high toxicity of Auger electrons is accredited to the highly localized energy deposition and formation of radical species in the immediate vicinity of the decay site. As a result, Auger electrons are in fact more advantageous in targeted therapy compared to β-particles because they deposit little or no radiation energy in non-targeted cells. Due to the greater depth of tissue penetration, β-particles has a higher non-specific toxicity and can adversely affect non-targeted cells that surround the tumour.

1.2 Choosing the best radionuclide for targeted therapy

For the most effective targeted therapy, the emitted radiation should be high linear energy transfer (LET) in nature and travel a short range inside tissue. Auger electrons fulfill these criteria and for efficient therapy planning, the biological effectiveness of these electrons has to be evaluated. Furthermore, a suitable radionuclide has to be carefully chosen for Auger electron therapy so as to ensure optimal radiation energy levels in treated cells. The selection of a radionuclide for therapy however, depends on many factors, including the type of tumour being treated (Bethge & Sandmaier, 2004). Basically, a high radionuclide accumulation and homogenous dose distribution would enhance rapid eradication of the target and spare normal tissue. Therefore, in choosing a suitable radionuclide, two aspects have to be considered, namely the dose and exposure time (i.e. dose rate) that depend on the half-life of the radionuclide. The following considerations should apply:

a) The half-life of the radionuclide has to be short enough so as to deliver a high radiation dose to the tumour in a short time. However, it should also be long enough to allow the radionuclide to be labeled to a suitable delivery agent and be taken up by targeted cells.

b) The exposure time to the patient should be short and can be achieved using a radionuclide with short half-life in order to prevent unnecessary radiation to the patient after treatment. A short half-life also allows for patients to be released from hospital soon after treatment without being troubled with radiation protection regulations – i.e. the patient is less contaminated by residual levels of radiation.

Iodine-123 meets the above requirements and was therefore selected as a suitable radionuclide. This isotope has a short half-life of 13.2 hours, and is readily available for research purposes as it is produced weekly at iThemba LABS for use in diagnostic medicine. Iodine-123 is produced mainly because it emits an almost ideal energy γ-ray (E_γ = 159 keV) that is frequently used in nuclear medicine applications.

The routine availability of an Auger electron emitter such as ^{123}I is a major advantage in the study of the biological effects induced by these electrons. In fact is very rare that a radioactive isotope with such a short half-life is used to study biological effects. More commonly used isotopes are those with longer half-lives – e.g. ^{125}I ($T_{1/2}$ = 60 days) – see below. The principal benefit from using ^{123}I is that with such a relatively short half-life, it becomes possible to accumulate sufficient numbers of disintegrations in cell cultures under normal physiological conditions (Slabbert *et al.*, 1999, Smit *et al.*, 2001).

1.3 Choosing the isotope delivery agent

The biological effects of high-LET Auger electrons are studied, as is often the case, relative to that from a low-LET reference radiation source. In this work, both the test and reference radiation emanate from the same source. This is possible because ^{123}I emits both Auger electrons (the test radiation) that travel in the nanometer range as well as energetic 159 keV gamma rays (the reference radiation). The latter serves to irradiate cells with low-LET radiation when applied in the form of a simple salt solution. In that way, the decay of the isotope is limited to the outside of the cell cytoplasm.

Since Auger electrons are in the nanometer range, decay of the radionuclide has to be within the cell nucleus so as to study their high-LET characteristics. For this, a suitable radionuclide carrier has to be employed. In this work, antipyrine (phenazone) was used. Phenazone is a lipid-soluble compound and hence can carry ^{123}I past the cytoplasmic and nuclear membranes to reach nuclear DNA. The radionuclide, therefore, deposits all its energy in the vicinity of the DNA upon decay (Miyazaki and Shinohara, 1993). Antipyrine is an organic compound that does not bind to DNA, but is located in part somewhere very close to the DNA and as such, ion radicals can move homogenously around the sensitive DNA target (Kassis *et al.*, 1999, Miyazaki and Shinohara, 1993).

A disadvantage in using antipyrine is that some of the radioactivity to which cells are exposed is not effective in inducing Auger electron damage inside the cell DNA. Because not all of the antipyrine is within the cell DNA, the damage to the DNA is not exclusively due to direct high-LET ionization and some indirect effects may apply (Smit *et al.*, 2001).

1.4 Motivation for doing the study

Auger electron emitters used by most investigators to study the radiobiological effectiveness of these particles have, for the most part, been radionuclides with long half-lives – for example ^{125}I ($T_{1/2}$ = 60 days) (Kassis *et al.*, 1999, Hofer *et al.*, 1992). Long half-lives result in low dose rates and this is disadvantageous for a number of reasons. First, targeted cells can divide whilst being irradiated thus making the quantification of biological damage difficult. In fact, biological effects can be quantified only when special arrangements have been employed to ensure a high number of disintegrations within cells

so as to allow measurable biological damage. To achieve this, cell samples are frozen with the radionuclides in liquid nitrogen (-196°C) over periods of weeks (Walicka *et al.*, 2001, Hofer and Bao, 1995). The biological damage induced under such artificial conditions may well be different from that induced under normal physiological conditions. In particular, the relative difference in biological damage induced by high and low-LET radiation types may be different in the frozen state. As such, the relative biological effectiveness (RBE) of Auger electrons may significantly differ from those estimated to date and can therefore lead to erroneous conclusions. Secondly, radionuclides with relatively short half-lives deliver significant radiation doses in shorter periods, thus minimizing the influence of repair of sublethal damage.

Furthermore, the RBE of Auger electrons is expected to be different when measured under normal culture conditions. This is because the frozen state is expected to protect cells more against radiation damage from indirect action than from direct action. This assumption is based on the fact that radioprotection from radical scavengers such as DMSO is always more for cells irradiated in frozen state due to the significant reduction in the production and mobility of free radical species (Ntuane, 2000). As irradiations with isotopes with relatively long half-lives require that cells be frozen with dimethylsulfoxide (DMSO), the influence of such a strong scavenger of radicals must also be considered. When cells are irradiated at room temperature, free from the radical scavenging properties of DMSO, the production and mobility of radicals is expected to increase, and this may lead to more indirect damage.

The frozen state is also expected to inhibit the repair of cellular damage. Relatively more sublethal damage is induced by low-LET radiation and any lack of repair due to high-LET radiation, can be expected to be more pronounced in frozen cells. This in turn leads to an increased toxicity of low-LET radiation and will in principle, result in the reduction in RBE. Because high-LET radiation (alpha particles, neutrons) induces more direct damage to DNA compared to low-LET reference radiations (159 keV γ-rays for ^{123}I, ^{60}Co γ-rays), the RBE of high LET radiation is expected to increase. This study proposes to test this by irradiating cells with ^{123}I in the form of 4-[^{123}I]iodoantipyrine as test radiation and [^{123}I]NaI as reference radiation as well as ^{60}Co (low-LET). This in turn, supports the notion that cellular irradiation at normal physiological conditions using short-lived radionuclides is more advantageous than frozen state irradiations with long lived isotopes.

1.5 Purpose of the study

Ionizing radiation is particularly lethal to mammalian cells as it can cause the loss of reproductive capacity or even death. For such pronounced effects, the cell nucleus, which is the most critical target of ionizing radiation, has to be severely damaged. To achieve high levels of radiation dose delivery to the nucleus, the current study proposes the use of a suitable radionuclide that emits short ranged Auger electrons and exhibits adequate nuclear uptake. A possible candidate is ^{123}I.

The first part of this investigation was to synthesize a product that would be able to carry the radioactive ^{123}I into the cell nucleus without affecting the cellular kinetics. Unlike ^{123}I

from NaI that is naturally kept outside the cytoplasm as the cell membrane of most cell types is impermeable to [^{123}I]NaI (Kassis & Adelstein, 1980), the lipid-soluble properties of antipyrine enables it to pass the cytoplasmic and nuclear membranes to allow the decay of ^{123}I to occur in close proximity to the nucleus. Auger electrons from NaI can therefore not reach the nuclear DNA, and the low-LET 159 KeV γ-rays which are also emitted from ^{123}I, constitutes the reference radiation. The test radiation comprised of the Auger electrons from 4-[^{123}I]iodoantipyrine. Cells were exposed to either 4-[^{123}I]iodoantipyrine or [^{123}I]NaI, and the resulting cellular damage was quantified by the formation of micronuclei (MN). A major advantage in using the same isotope for both the low-LET and high-LET arms of the investigation is that one does not need to calculate the physical dose absorbed as a result of exposure, but can use the number of disintegrations that occur per unit volume of cell sample as a measure of dose.

To observe the biological characteristics of Auger electrons, cells of different radiosensitivities were exposed to the radionuclide in the two preparations indicated above. The purpose of this was to establish if the high-LET nature of Auger electrons (4-[^{123}I]iodoantipyrine) is such that it will result in less variations in cellular response compared to that by the reference radiation ([^{123}I]NaI). A reduced variation in micronuclei frequencies can be expected from the high-LET part of the study in a manner similar to that seen with neutrons and gamma rays (Theron *et al.*, 1997, Slabbert *et al.*, 2000). Also, test samples containing a radioprotector were treated with the two ^{123}I preparations to assess the nature of damage induced by Auger electrons.

CHAPTER II

2. Literature review

2.1 History of Auger electrons

Auger electrons were first discovered in 1925 by a French physicist, Pierre Auger, while investigating the pattern of electron tracks caused by low energy X-rays in a cloud chamber (Hofer, 2000). In his findings, he noted that in some cases multiple electron tracks originated from a point source in a cloud chamber. This effect is due to electron transitions that take place when low-energy X-rays impinge on target atoms and eject electrons from inner shells. The resulting vacancy cascades therefore led to the emission of characteristic X-rays, Auger electrons, Coster-Kronig and super Coster-Kronig electrons.

During his investigations, Auger also noted that the phenomenon only took place during electron capture (EC) and/or internal conversion (IC) decay modes of some radionuclides. Due to their pattern of emission, Auger electrons gained a definition of orbital electrons emitted following the excitation of atoms by an incident electron beam (Shard and Cowie, 1998). During a typical EC decay, an electron drops from the L_1-shell to fill a vacancy formed in K-shell ionization. The resulting characteristic X-ray with energy E_K-E_L may not be emitted from the atom, and can strike an electron from a higher sub-shell (e.g. L_2-shell electron). This electron is then ejected as a low energy Auger electron (Figure 2.1). By contrast, Coster-Kronig transitions involve two principal electron orbital shells. For example, an electron from a higher sub shell-L_2 fills a vacancy

in the L_1-shell and an electron from the higher electron orbital-M_1 is emitted. In the case of super Coster-Kronig transitions, only one principal energy orbital (M-shell) is involved. For this, the vacancy in the M_1 shell is filled by another electron falling from a higher sub-shell-M_2 and an electron is emitted from another higher sub-shell (M_3), all in the same major energy-M shell.

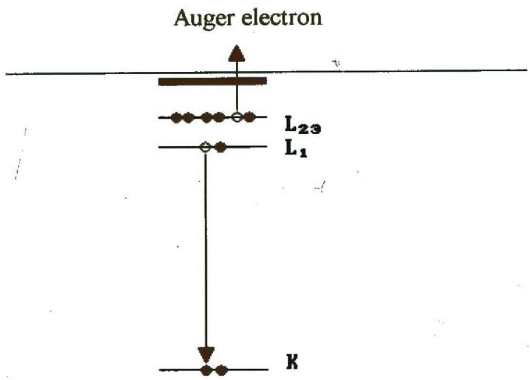

Figure 2.1 *Auger electron emissions.*

2.2 Biological significance of Auger electrons

For many years since the discovery of Auger electrons, their biological significance was not appreciated because of the fact that their low energy (<500 eV) was considered trivial compared to the total energy emitted by the decaying radionuclide. This misunderstanding continued until Charlson and White in 1964 reported that the decay of ^{125}I in methyl or ethyl iodide caused molecular fragmentation (Karagiannis 2003, Hofer 2000). This discovery led to numerous investigations including that the decay of ^{125}I labeled to the thymidine analog – iododeoxyuridine (IUdR), was found to be highly toxic to mammalian cells, and this toxicity was attributed to the Auger electrons emitted from

the charged daughter atoms in the immediate vicinity of the critical cellular target (Hofer *et al.*, 1992, Kassis *et al.*, 1987). It has previously been demonstrated that the high-LET nature of Auger electrons depends on the location of the decaying radionuclides (Slabbert *et al.*, 1999, Kassis *et al.*, 1999). Auger emitters located outside the cell nucleus are reported to be relatively non-toxic, whereas those that decay inside the nucleus cause high-LET type damage including DNA mutations, chromosomal aberrations, single and double strand DNA breaks and even cell death (Hofer *et al.*, 1992, Miyazaki and Shinohara, 1993).

2.3 LET and RBE relationship

Radiation types with different qualities have different degrees of effectiveness in producing biological damage in cells. Not only is the macroscopic dose (J/kg – units in Gy) important, but also the microscopic dose distribution - amount of energy absorbed per unit path length - determines the final level of biological damage. This microscopic dose distribution is referred to as linear energy transfer (LET). Ionizing radiation is classified as either low or high-LET. Low-LET radiation types are those that deposit their energies more uniformly in the cell volume with ionizations occurring relatively farther apart in a particular track. These include, among others, high energy X-rays, gamma rays, positrons and electrons. Conversely, those radiation types that deposit their energies more closely in a given radiation track are high-LET. Per unit dose, this type of radiation is more damaging and has more lethal biological effects than low-LET radiation. For example, normal tissue damage resulting from 20 Gy neutrons (mean energy 30 MeV) is about equivalent to damage caused by 60 Gy of 6 MeV X-rays (Sebeela, 2003). The total

distance in which a particle deposits its energy determines in part the ionization density. Auger electrons typically deposit their energies in the nanometer range. Therefore, although the energies of these particles are low, the ratio of hundreds of electron volts to nanometers yields a high ionization density of many 10's of keV/μm. This is comparable to the ionization density of other high-LET radiation types like neutrons (20 keV/μm) and alpha particles (100 keV/μm).

Most high-LET type radionuclides used in targeted therapy are alpha and Auger electron emitters. These particles have very different ranges in tissue with different relative biological effectiveness (RBE). The RBE for a given test radiation (e.g. α-particles or 4-[^{123}I]iodoantipyrine) is calculated as the ratio of the dose of the reference radiation (e.g. x-rays or [^{123}I]NaI) to the dose of the test radiation required to produce the same level of biological effect (Hall, 1998).

$$RBE = D_{ref} / D_{test} \quad (1)$$

where D_{ref} and D_{test} are the reference and test doses, respectively. Scientific investigations with these radionuclides have been conducted to assess the RBE of these radiation types under different experimental conditions, and in general RBE values serve as a useful way to compare the therapeutic potential of different treatment modalities including radionuclides.

For α-particles, β-particles and Auger electrons, the RBE values are expected to differ due to the different ionization densities of these particles. This in turn is determined by the energy and charge of the particle that also determines its range in tissue. The RBE values of Auger electrons are comparable to those of α-particles and can be as high as 10

(Gragg *et al.*, 1978, Sasaki 1984). RBE is influenced by many factors, including biological parameters such as the cell's inherent radiosensitivity and cell age, and physical factors such as dose and ionization density.

Radiation therapy with β-particles emitters is expected to be advantageous due to the relatively long range of β-particles in tissue. However, the greater penetration of β-particles results in pronounced biological damage to normal tissue as a result of the cross-firing effect. Also, the low-LET nature of these electrons necessitates the use of higher doses and longer exposure times during therapy. This restricts the use of β-particles in targeted therapy to treating relatively large tumours and not small metastatic diseases (Bethge and Sandmaier, 2004). Auger electrons and alpha particles therefore gain the advantage in tumour therapy for single cell kill and for targeting minimal residual diseases (MRD) or micro-metastatic lesions.

2.4 Radionuclides for medical use

Many radionuclides are used in nuclear medicine for diagnostic and therapeutic purposes. For successful therapy, the tumour cells first need to be located by imaging which provides access to measuring acute tumour responses to therapy trials prior to the implementation of radiotherapy for a specific tumour of an individual patient (Feinendegen, 1991). Some radionuclides used in nuclear medicine can be used for both imaging and therapy of metastatic tumours when labeled to suitable delivery agents. Table 2.1 lists the possible sources of Auger electrons, α- and β-particles used in nuclear medicine for both diagnostic and therapeutic purposes.

Table 2.1 Radionuclides suitable for diagnosis and/or therapy. E_{max} is the maximum particle energy and E_γ is the energy of the corresponding γ-component.

Radiation type	Radionuclide	Physical half-life	E_{max} [MeV]	Range in tissue	Eγ [MeV]
β^-	^{111}Ag	7.5 days	1.05	4.8 mm	0.342
	^{67}Cu	61.9 hours	0.57	1.8 mm	0.184
	^{131}I	8.0 days	0.81	2 mm	0.364
	^{177}Lu	6.7 days	0.50	1.5 mm	0.208
	^{32}P	14.3 days	1.71	8.7 mm	-
	^{186}Re	3.8 days	1.07	5 mm	0.137
	^{188}Re	17.0 hours	2.11	11 mm	0.155
	^{90}Y	2.7 days	2.27	12 mm	-
β^+	^{11}C	20 min	1.0	0.56 mm	0.511
	^{18}F	110 min	0.60	0.44 mm	0.511
	^{13}N	10 min	1.2	0.78 mm	0.511
	^{15}O	2 min	1.7	2.10 mm	0.511
α	^{211}At	7.2 hours	6.8	65 μm	-
	^{212}Bi	1.0 hour	7.8	70 μm	0.720
	^{225}Ac	10 days	5.8	60 μm	100
	^{213}Bi	45.6 min	-	70 μm	-
Auger	^{123}I	13.2 hours	0.03	10 nm	0.159
	^{125}I	60 days	0.03	10 nm	0.027
	^{111}In	2.8 days	0.03	10 nm	0.173, 0.247
	^{51}Cr	27.7 days	0.75	10 nm	-
	^{201}Tl	72.9 hours	0.48	10 nm	-
	^{64}Cu	12.7 hours	0.58	10 nm	-
	^{68}Ga	67.6 min	2.91	10 nm	-
	^{67}Ga	3.3 days	0.01	10 nm	0.090

At iThemba LABS, a number of radionuclides that emit Auger electrons are produced and in principle are available for use in radiobiological studies. These include ^{67}Ga, ^{68}Ga, ^{18}F, ^{111}In and ^{201}Tl. Thallium-201 is particularly interesting as it is produced for use in clinical cardiology and heart imaging. It also emits a high number of Auger electrons (31 per decay) and is readily taken up by cells without the need to be labeled to an organic molecule. In practice, however, the isotope is only produced on rare occasions and as such is not suitable for routine studies that require batches of high levels of radionuclides.

2.5 Diagnostic radionuclides used in targeted therapy

Diagnostic radioisotopes are chosen for their mode of decay. For example, radionuclides decaying by electron capture and isomeric transitions are appreciated because of the emission of gamma rays that can be detected by gamma cameras. For imaging, γ-rays with energies of 100 - 200 keV are the most suitable. ^{123}I (E_γ = 159 keV) is in fact produced for this reason.

Many imaging radionuclides are β^+- emitters and their importance is based on the production of 511 keV annihilation photons which assist in the acquisition of high resolution images of small tumours as well as quantitative evaluation of the distribution of radioactivity inside larger tumours (Bernhardt and Forssell-Aronsson, 2001). Auger emitters such as ^{67}Ga, ^{51}Cr, ^{201}Tl, ^{64}Cu and ^{68}Ga are also used for diagnosis. For instance the cyclotron-produced ^{67}Ga is used in single photon emission computer tomography (SPECT) for detection and localization of tumours and lesions as well as imaging of abdominal infections. ^{68}Ga is a generator-produced radioisotope used in PET imaging due

to its non-halogen and non-volatile chemical properties. Its 68-minute half-life permits chemical manipulation for the production of many PET radiopharmaceuticals. This radioisotope from its parent nuclide, germanium-68 and is used in PET to study thrombosis. These diagnostic radionuclides (^{67}Ga and ^{68}Ga) can also be labeled to peptides to target liver cancer cells.

Some Auger electron emitting radionuclides can be used for therapeutic or diagnostic purposes or both. For example, ^{99m}Tc, having a three-step de-excitation to ^{99}Tc by IC transitions and an emission of 140 keV γ-ray, is suitable for imaging of metastatic disease as well as for their therapy. Also, the production of this Auger emitter by using a ^{99}Mo/^{99}Tc generator makes it possible for a wider use in nuclear medicine.

2.6 β-Emitters as a source of radiation for targeted therapy

Many β-emitters are used in nuclear medicine for tumour therapy and these include ^{90}Y, ^{89}Sr, ^{153}Sm, ^{32}P, ^{67}Cu, ^{131}I, ^{177}Lu, ^{186}Re and ^{188}Re. For example, radionuclides such as ^{89}Sr, ^{153}Sm and ^{186}Re are used for palliative therapy in bone cancer. These radionuclides are intravenously injected in the form of $^{89}SrCl_2$, ^{153}Sm-EDTMP (ethylene-diamine tetramethylene phosphoric acid) and ^{186}Re-HEDP (hydroxyethylene diphosphonate), respectively (Lamki, 2000). Like calcium, strontium is metabolically taken up in the bones. Similarly, ^{186}Re and ^{153}Sm are taken up like phosphates in the bones due to their phosphate moieties - HEDP and EDTMP. ^{153}Sm is also used for definite therapy of osteosarcoma rather than just pain relief.

Labeling of antibodies for cancer therapy is also a promising modality. For example, the Food and Drug Administration (FDA) has given permission during the last year to use ^{90}Y in cancer therapy (Bethge and Sandmaier, 2004). Yttrium-90 is a radiometal emitting high-energy (>2 MeV) β-particles, and can be labeled to monoclonal antibodies - CD20 for treatment of B-cell lymphoma. These monoclonal antibodies attach to the target antigen and carry with them the radionuclide into the genome of the target cells.

Govindan *et al.* studied the effectiveness of this radiometal together with ^{131}I-linked to CD74 antibody *in vitro* as therapeutic agents for B-cell lymphoma and compared this to that from Auger emitters ^{111}In, ^{67}Ga and ^{125}I (Govindan *et al.*, 2000). Their findings showed that β-emitters killed B-lymphoma cells when conjugated to antibodies, and that this cell killing resulted from greater depths of penetration of β-particles in tumours. However, higher levels of nonspecific toxicity were also noted. An advantage of the long ranged β-particles is that antigen negative cells that surround the tumour can also be irradiated. As compared to Auger emitters, circulating β-particles will deliver substantial radiation dose to the bone marrow whereas Auger electrons will deliver only minimal dose to non-targeted cells. Because of the longer ranges, β-emitters have an advantage in treating solid tumour masses since they have the ability to kill cells at some distance away from the emission site (Govindan *et al.*, 2000, Ochakovskaya, *et al.*, 2001, Bethge and Sandmaier, 2004).

Similar studies of β-emitters were conducted using ^{90}Y, ^{186}Re and ^{67}Cu to target CD19, CD20, CD22, CD37 and the major histocompatibility complex (MHC) antigens (Bethge

and Sandmaier, 2004). It was also found that antibody-labeled β-emitters had a greater potential for treating B-cell lymphoma. Other β-emitters like ^{131}I are labeled to MIBG to treat neuroblastoma and [^{131}I]NaI is used in the treatment of thyroid cancer.

2.7 α-emitters as a source of radiation for targeted therapy

Alpha emitting radionuclides such as ^{212}Pb, ^{210}Po, ^{212}Bi and ^{211}At are attractive for some therapeutic applications because of their high densities of ionization along linear tracks. Therefore, these radionuclides are theoretically more lethal to cancer cells, and in principle less radioactivity is required for therapy. The high-LET nature and short range of α-particles limits the ability of cells to repair DNA damage and are also effective in killing cells under conditions of hypoxia (Hall, 2000). An obvious disadvantage of α-particles in targeted therapy is that they require binding of a carrier to most cancer cells in a tumour or to their neighbours for irradiation of all cells (Volkert *et al.*, 1991). For instance, accelerator–produced ^{211}At is a halogen with chemical properties close to that of iodine (both Group VII elements). However, unlike iodine it cannot be directly labeled to organic compounds. Instead ^{211}At has to be conjugated to antibodies using a linker (Digvi, 2001). ^{211}At conjugates with monoclonal antibodies (Mabs) are currently being evaluated as potential therapeutic agents. In principle this isotope is almost ideal as it is an α-emitter with a short half-live (7.2 hours). Astatine-211-labeled Mabs and another α-emitter, ^{212}Bi, are employed in the treatment of leukemia or for use in specific target structures in body cavities such as the peritoneum (Volkert *et al.*, 1991)

2.8 Auger electrons as a source of radiation for targeted therapy

Most Auger electron research in radiation biology has been performed using ^{125}I (Kassis *et al.*, 1987, 1999, Hofer *et al.*, 1992, Miyazaki and Shinohara, 1993). This isotope is mainly labeled to thymidine analogs like 5-deoxyuridine. Due to the long half-life, easy de-halogenation and strong thyroid avidity, the use of ^{125}I as a source for therapy is limited (Humm and Charlton, 1989). To ensure sufficient accumulation of dose from ^{125}I with a half-life of 60 days, cells have to be exposed for relatively long periods. In most cases, the use of ^{125}I demands that cell irradiation takes place during storage in liquid nitrogen (Walicka *et al.*, 2001, Hofer & Bao 1995). Freezing cells requires the use of radiation protection and radical scavenging agents such as dimethylsulfoxide (DMSO) that may modify the cellular radiation responses. This is one of the principal reasons why ^{123}I is used in this study of the biological effect of Auger electrons.

2.9 Cellular effects of Auger electrons

As pointed out earlier, the mode in which Auger electrons cause biological damage depends critically on the location of the decaying radionuclide. Auger emitters incorporated into the nuclear DNA are expected to be highly toxic due to high-energy deposition at the decay site. Conversely, identical decay events taking place in the cytoplasm, plasma membrane or any other structure outside the nuclear DNA may be relatively non-toxic as most of the nanometer-ranged energy of Auger electrons is attenuated. Investigators using ^{125}I have established that Auger electron damage at the site of DNA is as toxic as that of alpha particles from ^{210}Po (Kassis *et al.*, 1987, Miyazaki and Shinohara 1993, Kassis *et al.*, 1999, Biyashee *et al.*, 2000). Although these

investigators used different biological end-points including micronuclei formations, surviving fractions, DNA single or double strand breaks and sperm-head abnormalities, the results showed higher toxicity for intracellular irradiation than for extracellular exposure.

2.10 The indirect action of Auger electrons in causing biological damage

For cell damage, the primary structure that has to be targeted is the cell nucleus, which is more sensitive to ionizing radiation. It is also evident that water forms about 70% of the cells' composition and constitutes the primary target that makes the cell more prone to radiation. Following absorption of any form of ionizing radiation, free ions are induced in the water component of the cell and a number of processes take place including physical, biochemical and biological processes (van Rooyen, 2003). For example, between 10^{-6} and 10^{-13} seconds after absorption of ionizing radiation, a host of radicals and other chemical species are formed in the water component of the cell. These species are extremely reactive and attack any molecule (including DNA) in their vicinity. They can also move rapidly in the medium some distance from their site of origin and cause further chemical changes in molecules before they are inactivated. These radicals can also react with other radicals or molecules to form a chain of $OH^{\bullet}$ radicals and other chemically reactive compounds. For example two $OH^{\bullet}$ radicals can react to form hydrogen peroxide i.e.

$$OH^{\bullet} + OH^{\bullet} \longrightarrow H_2O_2$$

This peroxide is extremely toxic to the DNA as it can attach to or cause the DNA to break up. During all these processes, direct and indirect effects of ionizing radiation take place (Figure 2.2). High-LET radiation sources such as neutrons and alpha particles mainly

cause direct damage. Interestingly, Auger electrons are high-LET radiation type but cause DNA damage mainly by indirect interaction. The major component of DNA damage from low-LET X-rays and gamma rays is also through indirect action.

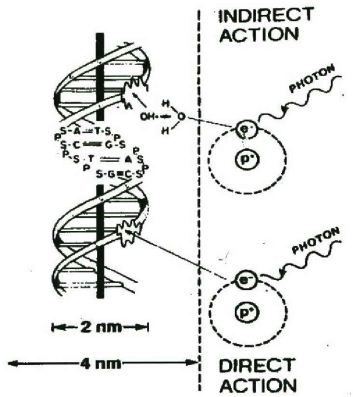

Figure 2.2 The indirect and direct actions of ionizing radiation in the nuclear DNA. The letters S, T, P, A, G and C represent sugar, thiamine, phosphorus, adenine, guanine and cytosine, respectively (Hall, 1998).

2.11 The use of radioprotectors during cell irradiations

Chemical protection against ionizing radiation has led to the development of efficient radioprotectors that significantly diminish radiation injuries in living organisms. It is also evident that these compounds are very effective when administered before irradiation so as to reduce the radiation dose to normal cells. Radioprotectors are mainly used in the protection of military personnel against accidental exposure of ionizing radiation from nuclear weapon detonations or weapon accidents (Grachev and Sverdlov, 1997). Most effective radioprotectors used by military personnel are aminothiols and their derivatives,

which include cysteamine, cystamine, AET (aminoethanisothiuronium bromide hydrobromide), WR-638 (cyctaphos) and WR2721 (amiphostine). Another efficient radioprotector is WR-1067 but is mainly marketed as rat poison because of its high toxicity.

Amiphostine is the most common drug used in radiotherapy. It is a phosphorothioate that is non-reactive until it is dephosphorylated by the enzyme alkaline phosphatase to yield an active metabolite WR-1065 (Nakamura *et al.*, 1987). Normal cells readily take up this metabolite and it protects by the scavenging of free radicals generated by ionizing radiation or chemotherapeutic agents such as alkylating agents. It is also rapidly taken up by normal cells after administration but penetrates tumours very slowly, and the effective dose in normal cells is significantly reduced.

Cysteine and cysteamine were the first radioprotectors discovered in 1948 by Pratt and Bacq, respectively (Hall, 2000). These compounds consist of the sulfhydryl and the amino groups at each end of the molecule. The chemical representation of cysteamine is shown below.

NH_2-CH_2-CH_2-SH

Although cysteamine is an efficient radioprotector, it is also toxic to cells and causes nausea and vomiting at doses required for radioprotection. The toxic effects of cysteamine can however be modified by covering the SH group by a phosphate group. The chemical representation of cysteamine-PO_3 is:

NH_2-CH_2-CH_2- SH_2PO_3

When the radioprotector is administered prior to irradiation, a larger radiation dose is required to produce the same response than when the compound is not present. The ratio of the dose for a given response in the presence and absence of the radioprotector is called the dose reduction factor (DRF). Cysteamine is used in this study to assess the high-LET effect of Auger electrons in different cells with different radiosensitivities.

Chemical protectors cannot modify cellular damage caused by many high-LET radiation sources. (Hofer and Bao, 1995, Bishayee, *et al.*, 2000). However, Auger electron damage which is indirectly ionizing can be minimized by radioprotectors.

CHAPTER III

3. Materials and methods

3.1 Production of ^{123}I

The routine availability of ^{123}I at iThemba LABS is one of the main reasons for using this isotope to study Auger electron damage in cells. The following is a short description of the routine production of the isotope at iThemba LABS.

I-123 is produced via proton bombardment of a NaI target. In this the parent-daughter pair ^{123}Xe ($T_{1/2}$ = 2.08 hours) / ^{123}I ($T_{1/2}$ = 13.2 hours) is generated. It is thus imperative that after target bombardment, the ^{123}Xe parent be separated from the target material as quickly as possible because it is rapidly decaying to its daughter (the product nuclide), ^{123}I. This is accomplished by dissolving the aluminium encapsulated NaI in a hot solution of 2.5 M NaOH. The capsule is designed with a thinner band around a part of its circumference that preferentially dissolves, to allow the salt to go into solution and release the gaseous parent.

Since hydrogen is generated by the reaction of the base and aluminium, the radioactive xenon is driven on a gas stream through a condenser, then a secondary drying trap, and finally into a pair of stainless steel coiled traps, which are cooled in liquid nitrogen (b.p. -198.8°C). This is where ^{123}Xe (m.p. –111.8°C) is frozen out from the gas stream. It is important that the flow-rate is kept below 6 L/hr to ensure that the entire radioactivity is trapped. Gas passing through the coils is trapped and stored in a series of rubber

bladders. This provides a completely closed system essential in the case of a failure to trap the gaseous radioactive parent.

After a minimum of two ^{123}Xe half-lives (about 4 hours), the coils are removed from the liquid N_2 and heated up to room temperature (20°C). Undecayed radioactive xenon is then flushed to the storage bladders with a stream of helium. The product, ^{123}I, is then washed out of the traps with two small volumes (±5 ml) of 0.01M NaOH. Typically, the distribution of the product radioactivity between traps 1 and 2 is 98% : 2%.

Figure 3.1 below shows the decay of the parent and the growth of the daughter (log of the individual activities based on a start ^{123}Xe activity of 37000 MBq (1000 mCi)) as a function of time. It illustrates how rapidly the parent decays to the daughter and consequently the need for completing the separation as speedily as possible. It can also be seen that after 6.584 hours, the activity of the daughter, ^{123}I, has reached its maximum. At this point, the rate of formation of ^{123}I is equal to its rate of decay and there is therefore no added benefit to allow the parent to continue to decay after this period. For purpose of this study, a 5.5-hour decay period was chosen as it allows a decay conversion of ^{123}Xe to ^{123}I of 84%. Figure 3.2 illustrates the percentage decay of the parent radionuclide with respect to time.

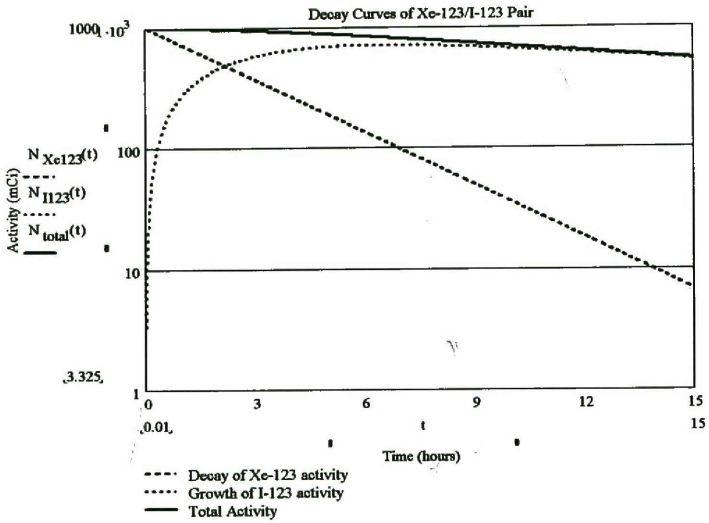

Figure 3.1 The decay of parent nuclide (^{123}Xe) and growth of daughter nuclide (^{123}I) as a function of time.

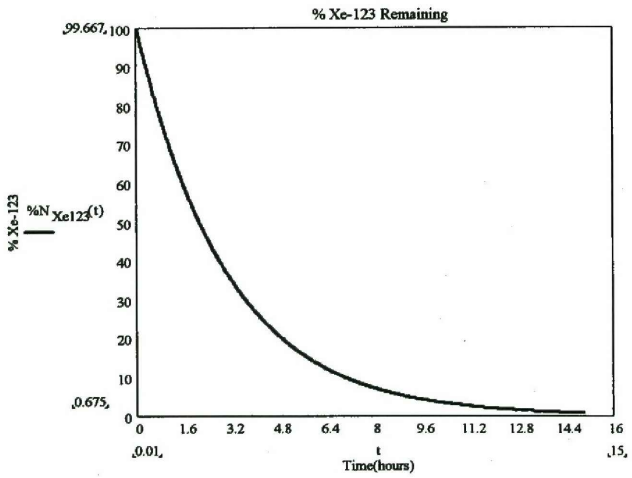

Figure 3.2 The percentage decay of ^{123}Xe with respect to time.

3.2 Synthesis of a delivery agent 4-iodoantipyrine

The diagram below represents the synthesis of 4-iodoantipyrine from antipyrine and NaI, using chloramine-T as an oxidizing agent and radiolabeling from [^{123}I]NaI using isotope exchange methods.

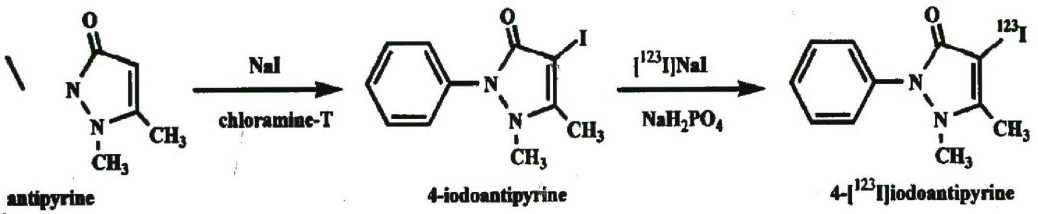

Figure 3.3 A schematic diagram representing the chemical reaction between Antipyrine and NaI to produce 4-iodoantipyrine and the radiolabeling with ^{123}I to produce 4-[^{123}I]iodoantipyrine.

4-iodoantipyrine, the cold substrate used in producing 4-[^{123}I]iodoantipryine, is not readily available and cannot be purchased commercially. Therefore it was necessary to synthesize the compound and for this the following procedures were employed. 500 mg antipyrine (phenazone) and 440 mg sodium iodide were dissolved in 12 ml water using a small (25 ml) conical flask (Quickfit). The solution was heated on a hot plate with continuous stirring until it reached 80°C. Then chloramine-T (822 mg) was added in 8 – 10 fractions for ten minutes. With every addition of chloramine-T, the solution turned yellow but the colour disappeared fast. Then a water-cooled condenser was attached to the conical flask and the solution was refluxed for 30 minutes with the stirrer running but the hotplate switched off. During this time a yellowish precipitate of 4-iodoantipyrine

formed around the mouth of the conical flask. This precipitate was filtered off using filter paper fitted into a Büchner funnel. The filtration was assisted using vacuum. The precipitate was then thoroughly washed with water followed by re-crystallization from 90% ethanol. This was left for several hours to allow the formation of yellowish crystals. To obtain pure crystals (white), the product had to be re-crystallized (filtered and dissolved in ethanol) at least five times. The purity of the final product was confirmed by a high performance liquid chromatography (HPLC) and the melting point technique. The melting point of the final product was found to be 164°C and was within experimental uncertainty comparable to the reported melting point of 4-iodoantipyrine (161.0 - 161.5°C) (Slabbert *et al.*, 1999).

3.3 Chromatogram analysis

The analysis of the purity of the final product was performed using Waters (Model 510) chromatograph (HPLC) equipped with a NaI(Tl) detector plus Ortec electronics (Figure 3.4).

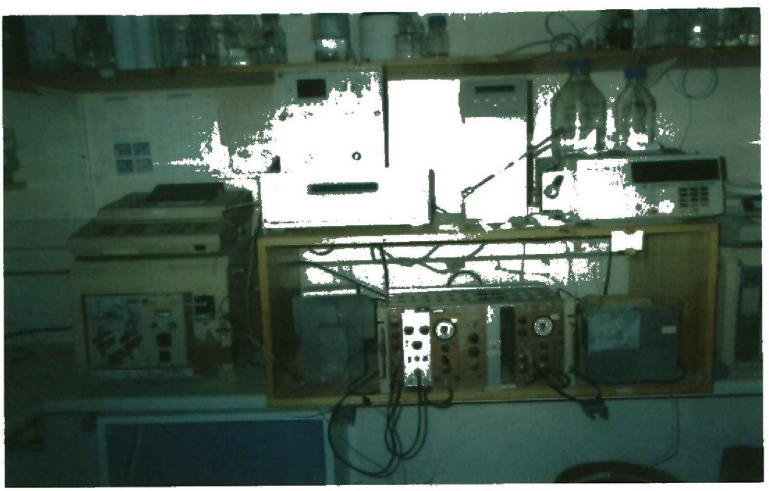

Figure 3.4 HPLC electronics

For the analysis, a chromatogram was run by first preparing the eluent and elute as follows:

a) Eluent preparation

An eluent solution was prepared by dissolving 0.05 M NaH_2PO_4 in 40 ml acetonitrile, 135 ml methanol and 325 ml distilled water on a magnetic stirrer. The pH of the final solution was then adjusted to 7 by adding drop-wise 20% tetrabutylammonium-hydroxide. The solution was run in a 30 cm C18 Spherex 5 column connected to the electronics.

b) Elute preparation

A few crystals of 4-iodoantipyrine were dissolved in about 400 µl of methanol. Of this, 5 µl was injected into the HPLC and run at a flow rate of 1.2 ml/min. Undissolved (free) iodine was eluted at 2.3-2.9 minutes and 4-iodoantipyrine at 5.6-5.9 minutes.

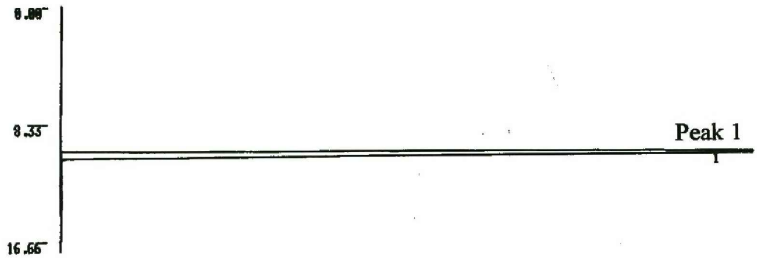

Figure 3.5 A chromatogram showing 100% 4-iodoantipyrine (peak 1) after repeated crystallization.

The result shown in figure 3.5 is that of the final 4-iodoantipyrine crystals following repeated re-crystallizing. HPLC analysis before repeated re-crystallizing showed multiple peaks indicating the presence of impurities – data not shown. The synthesis above yielded about 93.5 mg of substrate that was then used in the routine labeling with ^{123}I.

3.4 Radioactive labeling by ion exchange

3.4.1 Preparation of 0.1 mg 4-iodoantipyrine reaction vials

The reaction was carried out in a 2 ml glass vial containing 0.1 mg well-dried 4-iodoantipyrine. Since it is not possible to accurately weigh 0.1 mg of 4-iodoatipyrine, a stock solution was prepared first by dissolving accurately weighed 1.2 mg of 4-iodoantipyrine in 600 µl chloroform. Twelve 2 ml vials each received 50 µl of the chloroform solution. Then the chloroform was evaporated (boiling point 60°C) by placing the vials for 2 hours in an oven set at 70°C, leaving the 0.1 mg of 4-iodoatipyrine

at the bottom of each vial. The vials were placed in a beaker, covered with parafilm and stored on a shelf for routine use. In each radioactive labeling, one vial was used.

3.4.2 Reaction mixture

The principle of the method behind ion exchange reactions is to mix a small amount of radioactivity with a relative large amount of antipyrine. In this method, the cold iodine on the ring is replaced with a high degree of efficiency with a radioactive ^{123}I. Here, a phosphate buffered solution was prepared by dissolving of 69 mg of NaH_2PO_4 (MW = 137.99) in 1 ml of fresh deionised water and 50 µl of the buffer solution were transferred into one of the vials containing 0.1 mg 4-iodoantipyrine followed by the addition of 150 µl of ^{123}I (activity about 270 mCi/ml). The total activity in the vial (about 40 mCi) was then capped and heated in a water bath at 100°C for 40 minutes, and 200 µl of deionised water were then added to the vial to increase the volume followed by heating for an additional 3 minutes.

3.4.3 Purification column

Before the exchange reaction was started, a resin column was prepared to purify the product. This purification column was prepared by adding 0.2 - 0.3 ml of wet AGMP-1 resin in a 3 ml syringe. This small column was plugged with cotton wool, clamped on a retort stand and then washed with 3 - 4 ml of fresh deionised water. When the exchange reaction was completed, the reaction mixture was collected with a blunt-tipped syringe and transferred to the top of purification column. Four elution fractions were collected as shown in figure 3.6.

Figure 3.6 Purification column and 4 elution fractions.

Fraction 1

Vial 1 was placed under the column to receive the eluate from the reaction mixture that drips through under gravity. Then the column was washed with 200 µl of water into the vial.

Fraction 2

The resin was eluted with another 200 µl of water and eluate was collected in vial 2.

Fraction 3

An eluate from 1000 µl of deionised water was received in vial 3.

Fraction 4

The resin column was finally washed with 500 µl of water and the eluate was collected in vial 4.

When the elusions were completed, the radioactivities in all vials as well as the column were measured in an activity counter (Isocal II- Radionuclide Assay Calibrator) as shown in figure 3.7. This activity counter is calibrated by the CSIR using National Standards.

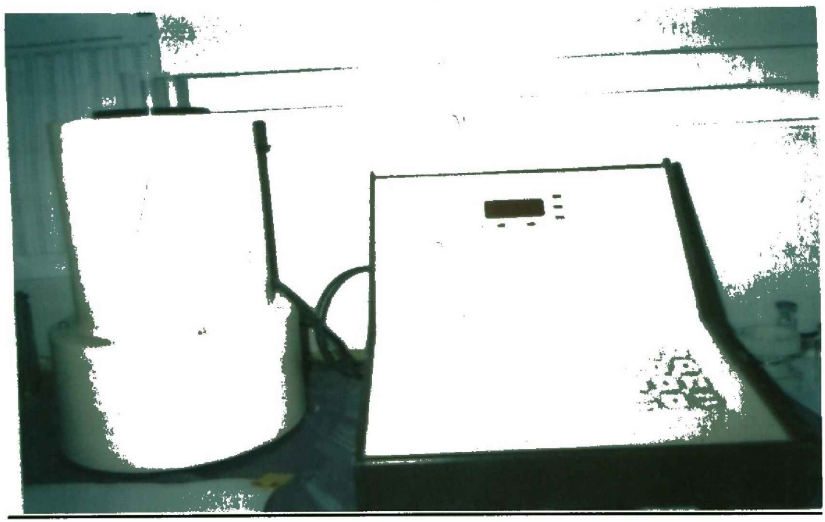

Figure 3.7 Activity Counter.

For cell irradiation, small quantities (~microlitres) of activity were used. This required the activity of the labeled compound to be as high as possible (preferably > 96%). Also, the amount of unbound ^{123}I should be small (< 5%) so that the quantification of biological damage in cells is predominantly due to the ^{123}I labeled to the organic molecule. To ensure this, only fractions having the highest activity were used and those with high levels of unbound ^{123}I discarded. Fractions containing the highest activities – usually fractions 3 and 4 were pooled for cell irradiations.

3.5 Preparation of labeled 4-[^{123}I]iodoantipyrine and unlabeled [^{123}I]NaI for cell irradiations

Given the specific activities that can be obtained with this labeling procedure, it became clear that relatively large volumes of up to 200 µl of labeled compound were needed to irradiate small volumes (~1 ml) of cell suspension. As 4-[^{123}I]iodoantipyrine and [^{123}I]NaI were collected in water, it was likely that the addition of the radioactive solution to cell suspensions would result in changes in culture conditions (e.g. pH and osmolarity). Therefore, the radioactive solutions were modified by adding the powdered form of growth medium corresponding to the cell line in question. The amount of media and bicarbonate of soda used were determined by the volume of the radioactive solution. The final liquid preparations of 4-[^{123}I]iodoantipyrine and [^{123}I]NaI were then sterile-filtered using a 0.22 µm-gauge filter. The volume of the final preparation added to the cell suspension depended on the activity at the end of the filtration.

3.6 Radioactivity measurements for labeled and unlabeled compounds

Following filtration, the radioactivities of the reagents (4-[^{123}I]iodoantipyrine and [^{123}I]NaI) were again measured since there was a possibility that some radioactivity may be retained in the disposable filter assembly. Appropriate volumes were then dispensed into the cell cultures. The mass of an empty 10 ml vial was first determined and again when the final preparation was added to it. The difference is an accurate measure of the volume and this is used to read off a volume correction factor that in turn is used by the activity counter.

3.7 Cell types, storage and culture maintenance

3.7.1 Cell types

In this study, four different cell types were used, namely, Chinese hamster ovary cells (CHO-K1) clone numbers #7 and #16, CHO-XRS 1 cells and human T-lymphocytes. The CHO cells were grown in T-25 tissue culture flasks as monolayers and lymphocytes were stimulated in suspension in round bottomed test-tubes. Cultures were incubated at 37°C in the presence of 5% CO_2 with the caps of the culture flasks and test tubes loosened to allow gaseous exchange.

i) Chinese hamster ovary (CHO-K1) #16 cells

These cells were a gift from Medunsa University (South Africa) and have been cultured over many years in the radiobiology laboratory at iThemba LABS. The cells were cultured in α-modified minimum essential medium (α-MEM) supplemented with 10% fetal bovine serum (FBS) and the antibiotics penicillin and streptomycin.

ii) Chinese hamster ovary (CHO-K1) # 7 and CHO-XRS 1 cells

These cell lines were kindly provided by Dr A. Serafin (University of Stellenbosch, South Africa), and are essentially the same as clone #16. However, they are listed separately as they are known to be considerably more radiosensitive than the CHO-K1 #16 clone. Clone # 7 cells were also cultured in α-MEM supplemented with 10% FBS. The CHO-XRS 1 cells are regarded to as a special repair deficient clone of CHO cells that are extremely radiosensitive, and hence the designation XRS. They were maintained

in α-modified minimum essential medium (α-MEM) supplemented with 5% FBS. Both media contained 10% antibiotics - penicillin and streptomycin.

CHO cells have a high plating efficiency and a doubling time of about 11 hours. This makes them suitable for all kinds of studies including survival using colony formation (Ntuane, 2000) as well as micronuclei formations.

iii) Human T-lymphocytes

The human lymphocytes used in this study were obtained from a single male donor. The cells were isolated from whole-blood samples using Ficoll gradient and cultured in RPMI-1640 medium supplemented with 15% heat inactivated FBS.

Compared to standard CHO cells, lymphocytes are expected to be relatively radioresistant and have been used previously in Auger electron studies (Slabbert *et al.*, 1999). Since T-lymphocytes are non-dividing at first, all cells are in a G_0 state and as result are equally sensitive to radiation. Micronuclei formation in these cells is well documented (le Roux *et al.*, 1998).

3.7.2 CHO cell storage and culture maintenance

Cells were subcultured by setting up 10 flasks from a single flask of cells. When confluent, the cells were trypsinized, centrifuged, resuspended in FBS and 10% dimethylsulfoxide (DMSO) and immediately stored in vials in liquid nitrogen (-196°C). For subculturing a clone, a method of "dry" trypsinization was used. First, the medium

covering the cell monolayer in the flask was discarded and the cells were washed twice with 2 ml of trypsin-EDTA. Trypsin is a proteolytic enzyme that facilitates the detachment of cells in a flask and it is derived from a beef pancreas. Similarly, EDTA aids with the adsorbance of heavy ions such as Mg^{++} and Ca^{++} involved in the attachment of cells to the growth substrate. After the second wash, the flask is placed in an incubator for 3 minutes to allow the cells to round up as a result of the enzyme-EDTA action. Cells were then loosened by tapping the flask on the palm of the hand and resuspended in 10 ml of the growth medium.

For subsequent cell culturing, a vial of cells (2 ml) was taken from the liquid nitrogen and thawed in a water bath at 37°C and mixed with 8 ml of growth medium. To remove the DMSO, cell suspension was centrifuged at 1000 revolutions per minute (rpm) for 10 minutes and the supernatant discarded. The resulting pellet was then re-suspended in 5 ml of growth medium, transferred to a 25 cm^2 culture flask and incubated.

3.8 Preparation of CHO-K1 #16 cells for irradiation with ^{60}Co γ-rays and micronuclei analysis

Three ampoules containing cells were taken straight from the liquid nitrogen tank and irradiated immediately with 3, 4 and 5 Gy of ^{60}Co γ-rays. After irradiation, cells still in the frozen state were thawed in a water bath (37°C) and the DMSO removed as described above. These were then resuspended in fresh medium and counted using a hemocytometer. For controls, ampoules were first thawed in a water bath, washed to remove DMSO, resuspended, counted and then irradiated. Samples were appropriately

diluted and 2 ml of cells suspension (50 000 - 60 000 cells) were transferred into the 30 mm petri dishes, each containing a microscope coverslip. Cytochalasin B was added to each culture at a final concentration of 2 μg/ml and the cultures were incubated for 24 hours. Cytochalasin B is a drug that modulates mitosis by arresting cytokinesis whilst allowing karyokinesis so as to render cells binucleated. The incubation time of 24 hours is sufficient to yield a binucleation of at least 50%. The media were then discarded and cells on the coverslips were fixed with 3:1 methanol: acetic acid for ten minutes, air dried and stained with acridine orange for micronuclei counting.

3.9 Irradiation of CHO cells with 4-[^{123}I]iodoantipyrine and [^{123}I]NaI

Semi-confluent cell cultures were trypsinized, re-suspended in growth medium and the cells were counted. From this, 1 ml samples were placed in round bottom tubes and various amounts of either the labeled compound (4-[^{123}I]iodoantipyrine) or [^{123}I]NaI were added. The tubes were placed in lead pots and incubated for periods that ranged between 16 and 20 hours. Following the incubation, the radioactive medium was removed by centrifuging the cell suspension and re-suspending the cell pellet in 5 ml medium. From each sample, between 50 000 and 60 000 cells were seeded in triplicate into petri dishes containing coverslips and cytochalasin B was added as before. The cultures were incubated for another 24 hours and then processed for micronuclei counting.

3.10 Irradiation of CHO cells in the presence of β-mercaptoethylamine (MEA)

An ampoule containing a stock concentration of 1.15 mg/ml of the radioprotector MEA was taken from the freezer and 168 μl of this added to 10 ml of growth medium to give a

final concentration of 25 mM of MEA. MEA increases the pH of the medium and this was compensated for by adding a few drops 1 M HCl. Cells were then re-suspended in this medium and appropriate levels of radioactivity were added. After incubating for 16 hours, the cells were washed twice by centrifuging and re-suspending of pellets in growth medium. A complete removal of MEA is necessary to avoid any interference with cell kinetics. The final cell suspensions were then plated for micronuclei formation as described above.

3.11 Identification and counting of micronuclei

Fixed, well-dried cells were stained with acridine orange. Acridine orange is a fluorescent stain that is used in many applications for quantitative analysis of nucleic acids and can differentiate between dead and live cells (Ntuane, 2000). For staining, coverslips were immersed in an acridine orange working solution for 1 minute and then rinsed in warm millipore water followed by de-staining in a buffer solution (pH 6.8). A drop of buffer solution was placed on a clean, dry microscope slide and the coverslip carefully mounted upside down. The edges of the coverslip were then sealed with nail polish to prevent the slide from drying. For best results, the slide has to be counted within the same day of preparation. Micronuclei counting took place on a Zeiss Axioskop microscope equipped with a FITC fluorescent filter. Figure 3.8 shows a section of cells stained with acridine orange, some of which express micronuclei. Scoring of micronuclei is based on the following criteria:

1. The scored micronucleus must have the same colour, shape, staining properties and must be located within the same cytoplasm as the main nucleus.

2. Its diameter should not be more than 1/3 of the size of the main nuclei.
3. The scoring was restricted to binucleated cells.

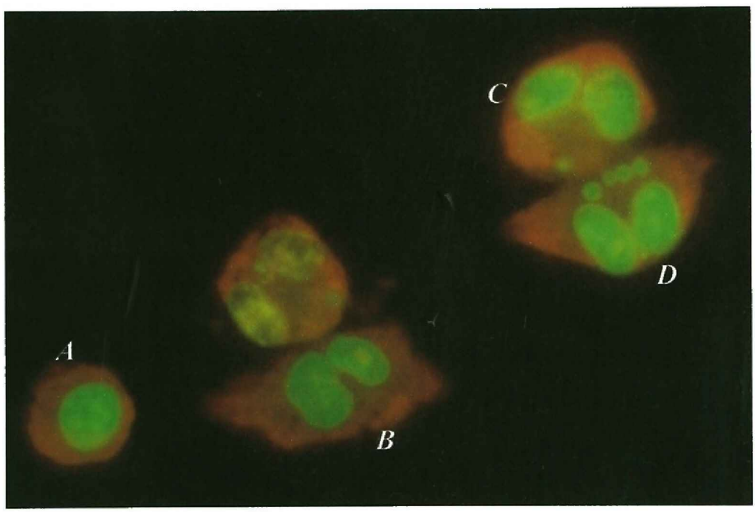

Figure 3.8 A slide of CHO cells showing a mononucleated cell (A), a binucleated cell with no micronucleus (B), one micronucleus (C) and four micronuclei (D) after a 16-hour exposure to 4-[^{123}I]iodoantipyrine (1.2 dist/μm^3).

3.12 Isolation of T-lymphocytes from a whole blood sample

For all trials, fresh whole blood samples were drawn into a 4.5 ml vac-u-test tubes with a purple cap containing the anticoagulant EDTA. To each blood sample, 2 ml sterile phosphate buffered saline (PBS) was added and mixed. This mixture was then carefully layered on 3 ml of Histopaque 1077 (Ficoll) in a volumetric test tube. This density gradient was then centrifuged for 30 minutes at 1000 revolutions per minute. After centrifugation, three layers were observed. The top layer was a serum/PBS mixture

whereas the middle layer contained a cloud of lymphocytes. Red blood cells settled at the bottom of the tube. The serum/PBS layer was discarded and the lymphocytes were removed and added to 5 ml sterile PBS and centrifuged for 10 minutes at 1000 rpm to wash out any Ficoll that may be present. The resulting supernatant was discarded and a pellet of lymphocytes at the bottom of the test tube was resuspended in RPMI-1640 medium supplemented with 15% FBS. A sample of lymphocytes for irradiation was typically that from about ½ of a 4 ml whole-blood sample.

3.12.1 Lymphocyte irradiation and culturing

Between 50 and 200 µl of 4-[^{123}I]iodoantipyrine or [^{123}I]NaI were added to 1 ml lymphocyte samples in round bottom test tubes. Samples were placed in lead pots and incubated for between 16 and 20 hours. The irradiation time was determined by the specific activity that applied to a particular preparation. Following irradiation, the radioactive medium was removed by centrifuging the cell suspensions at 1000 rpm for 10 minutes and discarding the supernatant. The cells were then re-suspended in 5 ml growth medium (RPMI-1640) supplemented with 15% FBS. To this, 50 µl of phytohemagglutinin (PHA) was added in order to stimulate cell division followed by incubation for 44 hours. Cytochalasin B was then added to the lymphocyte suspension and this was incubated for a further 28 hours in order to allow cells to be arrested in a binucleated state.

3.12.2 Lymphocyte fixing and slide preparation for micronuclei counting

Following culturing, cells were fixed for micronuclei counting. For this, cell suspensions were centrifuged at 1000 rpm and all but about 1 ml of supernatant were removed by vacuum suctions. This was then mixed with 4 ml of 75 mM of KCl while vortexing. The KCl was then removed by centrifuging at 8000 rpm for 8 minutes and again discarding all but 1 ml of supernatant. To this, 4 ml of fixative (3:1 methanol: acetic acid) were added while vortexing and samples were stored in a refrigerator (4°C) until used. The cell suspensions were then centrifuged at 800 rpm for 8 minutes and all but about 0.5 ml of fixative was removed. After resuspending the cell pellet with a pipette, three to four drops of the concentrated suspension were placed on a clean microscope slide and left to dry. From each lymphocyte suspension, at least four slides were prepared for micronuclei counting.

Well-dried slides were stained with acridine orange for 1.5 - 2 minutes, rinsed with millipore water and de-stained in buffer solution (pH 6.8). Coverslips were then mounted on the microscope slides and the edges were sealed with a nail polish to prevent it from drying, and the frequency of micronuclei formation assessed.

3.13 Radiation dosimetry

In this work, biological data is related to the number of disintegrations of ^{123}I that take place in a given volume of cell suspension. This is determined by the activity added and the time of incubation. The initial number of radioactive ^{123}I atoms, N_o, is given by:

$$N_o = A_o/\lambda \qquad (2)$$

where A_o is the initial activity and λ is the decay constant, $\lambda = ln2/T_{1/2}$. $T_{1/2}$ is the half-life of ^{123}I (13.2 hours). After incubating cells with an initial activity of N_o for t hours, the number of radioactive ^{123}I atoms left can be calculated using:

$$N_t = N_o . e^{-\lambda t} \qquad (3).$$

The difference between N_o and N_t represents the number of disintegrations that has taken place in the volume of cell suspension. For convenience, the number of disintegrations is expressed per micrometer cubed (μm^3).

The dose was expressed as the number of disintegrations per unit volume, since the physical dose of radiation energy absorbed is directly related to the number of disintegrations. Therefore, it is not necessary to calculate the dose in units of gray (J/kg) as the reference ([^{123}I]NaI) and test (4-[^{123}I]iodoantipyrine) radiations are performed with the same radionuclide.

CHAPTER IV

4. Results and discussions

4.1 Ion exchange reaction results

A total of 5 preparations were made during the course of this work and were used to investigate Auger electron damage in different cell types and under different physiological conditions. To evaluate the labeling process, results obtained on various preparations are listed below.

4.1.1 Run #1: first radiolabeling - 12 May 2004

Using the procedures detailed in materials and methods, the first labeling was made to test the suitability of the protocol. Radioactivity readings in different fractions collected from the purification column are listed in Table 4.1. In measuring the radioactivity, a factor is entered into the activity counter that corrects the reading for volume of the radioactive product in the 10 ml vial and the specific isotope in question.

A major shortcoming in this first labeling is the fact that most of the radioactivity (~25.73 mCi) placed on top of the resin column did not elute into any of the fractions collected and remained in the purification column. This was a result of using cold water for the elusions and it was suggested that boiling deionised water be used in subsequent runs.

Table 4.1 Measured activities of 4-[^{123}I]iodoantipyrine for each fraction collected from the purification column.

Elusion fraction	Activity (mCi)	Time of measurement	Decay correction factor	Reference activity (mCi)	Labeling efficiency (%)
1	0.210	14H15	0.3178	0.067	-
2	0.596	14H15	0.3178	0.189	-
3	5.317	14H16	0.3205	1.704	100
4	3. 632	14H16	0.3205	1.164	98.9
Column	25.73	14H19	-	-	-

Fractions 1 and 2 were considered unsuitable for use in cell experiments, as the labeling efficiencies were less than 95% as detected by HPLC analysis (Figures 4.1). The first two fractions contained less than 1 mCi of activity out of a total of more than 35 mCi added to purification column, indicating high levels of unbound radioactivity, and were thus discarded (Table 4.1.)

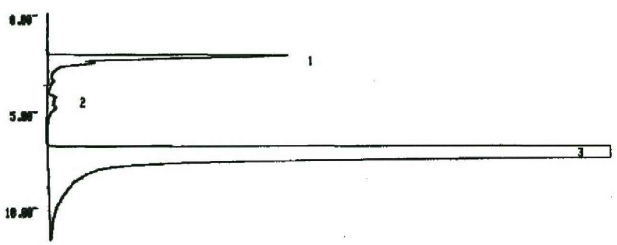

Figure 4.1 The labeling efficiency of fraction 1 as determined by HPLC. Peak-1 shows unbound ^{123}I to be more than 5%. Peak-2 indicates impurities that can be removed by filtration. Peak-3 shows that less than 95% of the antipyrine is labeled with ^{123}I.

The HPLC analysis of the third and fourth fraction collected from this labeling is shown below (Figures 4.2 and 4.3).

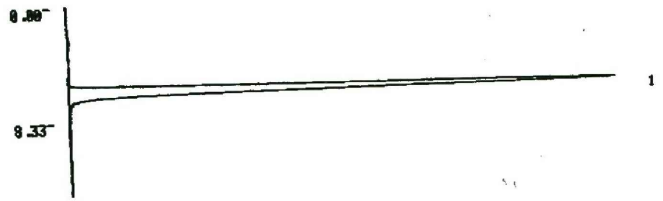

Figure 4.2 The labeling efficiency of fraction 3 as determined by HPLC. The single peak indicates that 100% of the antipyrine is labeled with ^{123}I.

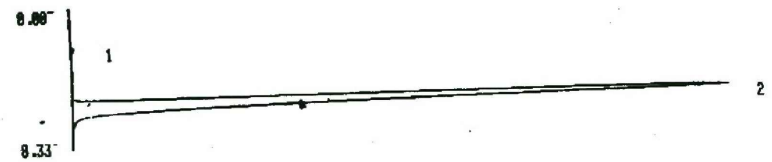

Figure 4.3 The labeling efficiency of fraction 4 as determined by HPLC. Peak-1 shows that 1.1% of the radioactivity was unbound and peak-2 represents the 98.9% antipyrine labeled with ^{123}I.

The fractions with the highest activities (3 and 4) were combined and their total activity was measured to be 8.240 mCi. From the readings of individual fractions, expected value was 8.949 mCi. The lower activity measured is possibly due to the difficulty in transferring one fraction to the other.

Following the addition of powdered growth medium and filtrating the radioactive solution, the final activities of both 4-[^{123}I]iodoantipyrine and [^{123}I]NaI were measured and the data is listed in Table 4.2. This final measurement was necessary since it is possible for the filter gauge to retain some radioactivity. Another reason for a reduction in activity is the decay that occurred during media addition and filtration.

Table 4.2 Radioactivities measured for the final 4-[^{123}I]iodoantipyrine and [^{123}I]NaI preparation.

	4-[^{123}I]iodoantipyrine	**[^{123}I]NaI**
Activity (mCi)	7.930	8.102
Volume (ml)	1.497	1.473
Specific activity (mCi/ml)	5.298	5.500

4.1.2 Run #2: second radiolabeling - 18 May 2004

The exchange reaction took place as in run #1 but elusions were performed using boiling deionised water. This resulted in more radioactivity being removed from the column, as reflected by the relatively low residual activity in the column (Table 4.3).

Fractions 3, 4 and 5 were combined because they had the highest activities and high purity - ranging between 97 and 98%. Fractions 1 and 2 were not analyzed by HPLC and were discarded as they contained less ^{123}I activities. It is clear from this that the maximum activity is released within fractions 3, 4 and 5. Figure 4.4 is the HPLC spectrum for fraction 4.

Table 4.3 Activities measured in elusion fractions and labeling efficiency by HPLC analysis.

Elusion fraction	Volume (ml)	Activity (mCi)	Time of measurement	Decay correction factor	Reference activity (mCi)	Labeling efficiency (%)
0	0.00	41.2	12H10	0.2861	11.79	-
1	0.317	2.21	14H00	0.3150	0.71	-
2	0.2061	2.63	14H00	0.3150	0.84	-
3	0.4121	9.53	14H10	0.3178	3.002	97.8
4	0.4571	7.99	14H10	0.3178	2.52	98.9
5	0.4391	3.93	14H20	0.3205	1.25	98.8
Column	-	8.1	14H30	0.3234	2.62	-

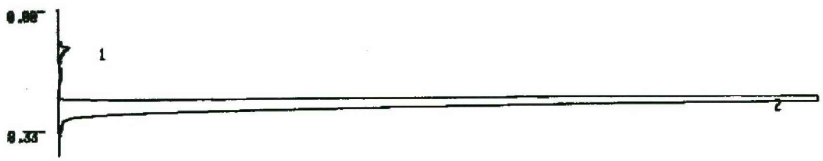

Figure 4.4 The labeling efficiency of fraction 4 as determined by HPLC. Peak-1 shows unbound ^{123}I to be less than 1.1%. Peak-2 shows ^{123}I bound to antipyrine to be 98.9%.

The activity of the combined product was then measured and was found to be 20.13 mCi (expected activity - 21.45 mCi). As this preparation was for the lymphocyte assay, RPMI-1640 medium was added to the two reagents (4-[^{123}I]iodoantipyrine and [^{123}I]NaI) prior to filtration and activity measurement, and the data presented in Table 4.4. The specific

activity using boiling water was about 3 times that of the first labeling, and supported this modification in the labeling protocol.

Table 4.4 Final activities of 4-[^{123}I]iodoantipyrine and [^{123}I]NaI after filtration.

	4-[^{123}I]iodoantipyrine	[^{123}I]NaI
Activity (mCi)	17.860	15.180
Volume (ml)	1.028	1.199
Specific activity mCi/ml	14.895	14.766

4.1.3 Run #3 : third radiolabeling - 24 August 2004

Results from this run were consistent with those observed in Run #2, and showed high activities (Table 4.5).

Table 4.5 Activities measured in elusion fractions and labeling efficiency by HPLC analysis.

Elusion fraction	Volume (ml)	Activity (mCi)	Time of measurement	Decay correction factor	Reference activity (mCi)	Labeling efficiency (%)
0	-	37.67	14H10	0.3178	11.970	-
1	0.460	3.39	15H20	0.3378	1.145	94.71
2	0.159	1.66	15H20	0.3378	0.559	-
3	0.935	11.90	15H30	0.3408	4.056	98.75
4	0.510	4.47	15H30	0.3408	1.523	98.55
Column	-	11.76	15H40	-	-	-

In this run, fractions 3 and 4 contained the highest radioactivities and purity (> 98%). These fractions were combined and their total activity was measured to be 12.06 mCi (expected activity - 16.37 mCi).

Figure 4.5 Chromatograph of fraction 4 showing 98.5% of antipyrine bound ^{123}I (peak 4) and 0.068% unbound ^{123}I (peak 1). Peak 2 and 3 shows some impurities that can be removed by filtration.

The activities of 4-[^{123}I]iodoantipyrine and [^{123}I]NaI after addition of medium and filtration were measured and shown in Table 4.6.

Table 4.6 Final activities of 4-[^{123}I]iodoantipyrine and [^{123}I]NaI after filtration.

	4-[^{123}I]iodoantipyrine	**[^{123}I]NaI**
Activity (mCi)	12.550	11.45
Volume (ml)	1.291	1.195
Specific activity (mCi/ml)	9.721	9.582

4.1.4 Run #4 : fourth radiolabeling - 12 October 2004

Data for this run are shown in Table 4.7. In this run fraction 2 unexpectedly showed a high level of radioactivity of 10.70 mCi, and was indeed the highest observed of all fractions collected. Also, fraction 1 had higher than usual labeling efficiency. The labeling efficiencies for these fractions were between 95 and 96% and as such were comparable with those of fractions 3 and 4. It was therefore necessary to compute the specific activities of all fractions to confirm which were usable. Despite the high labeling efficiency of fraction 1, it was discarded for its low specific activity. Fraction 2 was also not used since it showed a low labeling efficiency.

Table 4.7 Activities measured in elusion fractions and labeling efficiency by HPLC analysis.

Elusion fraction	Volume (ml)	Activity (mCi)	Time of measurement	Decay correction factor	Reference activity (mCi)	Labeling efficiency (%)	Specific activity (mCi/ml)
0	-	42.70	12H00	0.2836	12.109	-	-
1	0.480	2.48	13H50	0.3122	0.774	96.0	5.17
2	1.008	10.70	14H00	0.3150	0.3705	95.2	10.62
3	0.417	5.41	14H00	0.3150	1.703	96.1	12.97
4	0.483	4.75	14H00	0.3150	1.496	96.5	9.84
Column	-	12.33	14H10	-	-	-	-

Fractions 3 and 4 had lower activities than fraction 2 but their specific activities and labeling efficiencies were higher. They were therefore combined and the total activity was found to be 12.06 mCi (expected activity - 16.37 mCi).

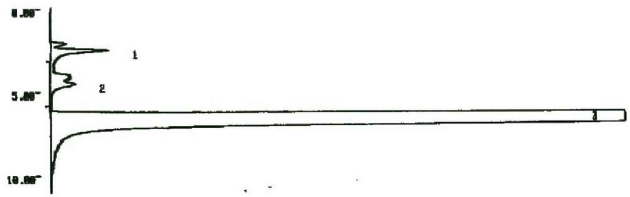

Figure 4.6 Chromatograph of fraction 3 showing 96.5% of antipyrine bound ^{123}I (peak 3). Only 1.7% was free ^{123}I (peak 1). Peak 2 indicates the presence of impurities that could be removed by filtration.

After the addition of α-MEM and filtration in both reagents, activities were measured and the data shown in Table 4.8.

Table 4.8 Measured activities of 4-[^{123}I]iodoantipyrine and [^{123}I]NaI after filtration.

	4-[^{123}I]iodoantipyrine	**[^{123}I]NaI**
Activity (mCi)	7.41	7.68
Volume (ml)	0.78	0.78
Specific activity (mCi/ml)	9.50	9.85

4.1.5 Run #5 : fifth radiolabeling - 09 November 2004

The measured radioactivities and purity of fractions collected are listed in Table 4.9.

Table 4.9 Activities measured in elusion fractions and labeling efficiency by HPLC analysis.

Elusion fraction	Volume (ml)	Activity (mCi)	Time of measurement	Decay correction factor	Reference activity (mCi)	Labeling efficiency (%)	Specific activity (mCi/ml)
0	-	40.23	13H00	-	-	-	-
1	0.5627	7.329	14H20	0.3205	2.349	93.7	13.030
2	0.2348	3.662	14H20	0.3205	1.174	95.8	15.596
3	0.9445	8.976	14H20	0.3205	2.877	97.3	9.503
4	0.4905	3.202	14H30	0.3234	1.036	98.3	6.528
Column	-	12.33	14H30	-	-	-	-

In this run, fractions 1 and 2 again had relatively high levels of radioactivity and the specific activities were the highest of all fractions. However, their labeling efficiencies were lower than those of fractions 3 and 4. As a result, fractions 1 and 2 were discarded. Fractions 3 and 4 were then combined and the net activity was measured to be 10.99 mCi (expected activity - 12.178 mCi).

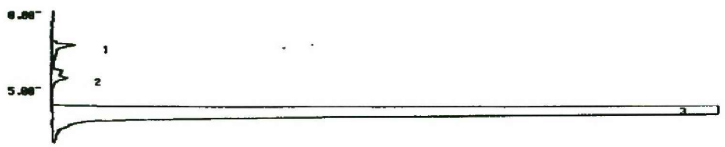

Figure 4.7 Chromatograph of fraction 4 showing 98.5% of antipyrine bound ^{123}I(peak 3) and 0.068% unbound ^{123}I (peak 1). Peak 2 shows some impurities that could be removed by filtration.

Following the addition of medium and filtration, the activities of the two reagents 4-[^{123}I]iodoantipyrine and [^{123}I]NaI were measured and the data listed in Table 4.10.

Table 4.10 Measured activities of 4-[^{123}I]iodoantipyrine and [^{123}I]NaI after addition of medium and filtration.

	4-[^{123}I]iodoantipyrine	**[^{123}I]NaI**
Activity (mCi)	10.03	9.211
Volume (ml)	1.372	1.274
Specific activity (mCi/ml)	7.310	7.230

4.1.6 Summary of labeling results

In all runs, relatively high efficiencies (> 96%) for labeling ^{123}I to antipyrine were obtained. The purity and stability of the 4-iodoantipyrine substrate were of high quality. It was concluded that by using the ion exchange reaction method (described in Chapter 3), ^{123}I can be labeled to antipyrine successfully to yield a product suitable for irradiating cells in culture. The low specific activity of 5.3 mCi/ml observed in Run #1 was

attributed to the use of cold water for the elusions. In runs 2 - 5, the mean specific activity was found to be 10.35 mCi/ml (range: 7.3 - 14.9 mCi/ml).

4.2 Results of cellular irradiation

4.2.1 Irradiation of CHO-K1 cells in frozen state and room temperature

As stated before, ^{123}I is used in these studies because it has a short half-life that allows cells to be irradiated without the need to freeze samples as reported by other investigators (Walicka *et al.*, 2001, Hofer and Bao, 1995). To appreciate the advantage of using ^{123}I, an experiment was first performed to assess the cellular damage resulting from irradiation in the frozen state and at room temperature. For this, CHO-K1 cell samples, either frozen or at room temperature were treated with 1 to 5 Gy of ^{60}Co gamma rays.

4.2.1.1 Frozen State Results

The results of cell samples taken from liquid nitrogen storage and irradiated without delay are listed in Table 4.11. Following irradiation, the cell samples were thawed to room temperature and cultures were set-up for micronuclei formation using the method described in Chapter 3.

Table 4.11 Micronuclei frequency distribution in binucleated CHO-K1 cells irradiated in frozen state.

Dose (Gy)	Total # of cells	0 MN	1MN	2MN	Total # of MN	MN/500 BN cells	% BN
0	625	618	7	0	7	5.60	62
3	827	783	41	3	47	28.42	51
4	1379	1295	80	4	88	31.91	51
5	339	307	27	5	37	54.57	41

4.2.1.2 Room temperature irradiations

Table 4.12 Micronuclei frequency distributions in binucleated CHO-K1 cells irradiated at room temperature.

Dose (Gy)	Total # of cells	0 MN	1MN	2MN	3MN	Total # of MN	MN/500 BN cells	% BN
0	625	618	7	0	0	7	5.60	62.0
1	1417	1352	63	2	0	67	23.64	52.9
2	1530	1406	119	5	0	129	42.16	43.5
3	1440	1265	161	14	0	189	65.63	40.9
4	1604	1325	246	31	2	314	97.88	40.1
5	1381	1085	255	36	5	342	123.82	30.8

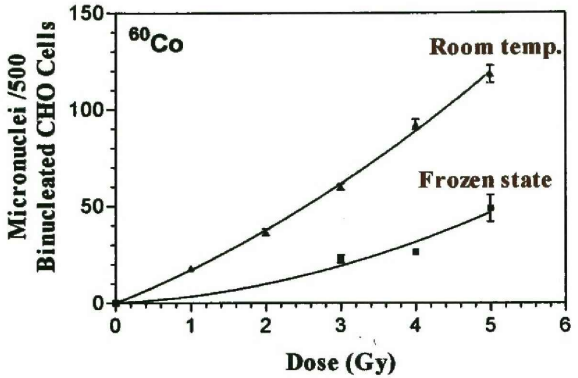

Figure 4.8 Dose response curves representing micronuclei frequency per 500 binucleated CHO-K1 cells irradiated with ^{60}Co at room temperature and in a frozen state.

The mean micronuclei frequencies observed in cells irradiated at room temperature or in the frozen state are plotted as a function of radiation dose in Figure 4.8. It is clear that the frozen state protect cells from radiation damage. The level of protection is high and a dose modifying factor (DMF) of about 2.5 can be estimated from the curves in Figure 4.8. The modifying factor observed in this study is significantly higher than that reported for CHO cells irradiated using X-rays at 37°C and –196°C (liquid nitrogen) by Hofer and Bao (1995). Using D_o values obtained from survival curves, a DMF of 1.6 was inferred. These investigators used 7% DMSO in freezing cells compared to 10% DMSO which was used in this study. Having a full set of surviving fraction data available, these investigators concluded that a modest DMF value of 1.6 is equivalent to a 3.2 fold increase in the radioresistance of cells.

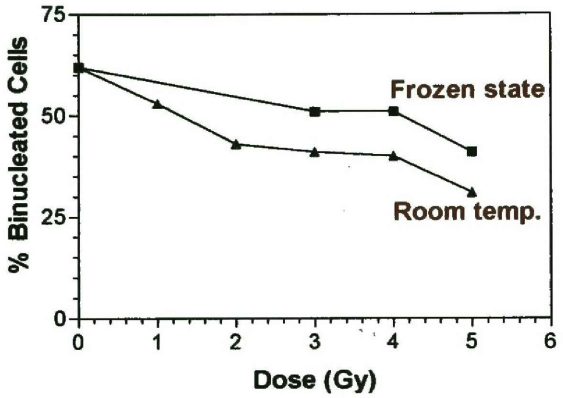

Figure 4.9 Percentage binucleation for CHO-K1 cells irradiated at different dose points at room temperature and in a frozen state.

The level of binucleation was also enumerated in these samples to follow the proliferative ability of cells (Figure 4.9). A systematic reduction in the percentage of cells that are binucleated with increasing dose is evident. This was expected, as increased mitotic delay is associated with more radiation damage. The higher levels of binucleation seen in cells irradiated in a frozen state confirm the radioprotective effect. In contrast, cultures irradiated at room temperature showed a lower level of binucleation and this is consistent with more damage per unit dose.

The high degree of protection seen in the frozen state is not surprising, as cells are protected from radiation damage by at least two distinctive mechanisms. First, the indirect effects of radiation are suppressed due to the radical scavenging properties of dimethylsulfoxide (DMSO) that is present. A second method of protection is that radicals

initiated by ionizing radiation may not readily migrate and as such not be effective in inducing indirect damage. It may be thought that the resulting damage in the frozen state irradiation is mainly from direct damage, which is mostly lethal. As such a linear dose-response curve could be expected. This expectation however, is not supported by the limited data in Table 4.11. The shape of the dose-response curve of the frozen state appears to be more linear–quadratic and thus similar to that of cells irradiated at room temperature.

From these results it is clear that it is indeed most beneficial to use ^{123}I to study Auger electron damage in cells. The level of biological damage reported in the literature by investigators who use radionuclides with long half-lives and need to freeze their cell samples is much lower than can be expected at 37°C using ^{123}I. What remains unresolved is if the frozen state has a differential effect on Auger electron damage compared to low-LET damage. To address this issue, Auger electron induced micronucleus yield was assessed.

4.3 Irradiation of CHO-K1 #16 cells with 4-[^{123}I]iodoantipyrine and [^{123}I]NaI

By adding between 50 and 200 µl of 4-[^{123}I]iodoantipyrine (specific activity: 5.298 mCi/ml) and [^{123}I]NaI (specific activity: 5.499 mCi/ml) to cell suspensions and incubating for 18 hours, the resulting number of disintegrations per unit volume are presented in Table 4.13.

Table 4.13 Cumulative doses (disintegrations per μm^3) of 4-[^{123}I]iodoantipyrine and [^{123}I]NaI to CHO-K1 #16 cells in suspension.

Volume added (µl)	**Disintegrations/µm^3**	
	4-[^{123}I]iodoantipyrine	**[^{123}I]NaI**
Control	0	0
50	0.391	0.406
100	0.747	0.775
150	1.072	1.112
200	1.369	1.422

The micronuclei yield corresponding to these doses are listed in Tables 4.14 and 4.15.

Table 4.14 Micronuclei yield and proliferation (% BN) observed in CHO-K1 binucleated cells treated with 4-[^{123}I]iodoantipyrine.

Disintegrations /µm^3	**Total # of cells**	**0MN**	**1MN**	**2MN**	**3MN**	**4MN**	**Total # of MN**	**MN/500 BN cells**	**% BN**
0	1094	1087	17	0	0	0	17	7.77	61
0.4	606	580	25	1	0	0	27	22.28	53
0.8	368	332	25	9	2	0	49	66.58	41
1.1	440	362	51	23	3	1	110	125	44
1.4	481	406	49	21	3	2	108	112.27	43

Table 4.15 Micronuclei yield and proliferation (% BN) observed in CHO-K1 binucleated cells irradiated with [^{123}I]NaI.

Disintegrations / μm^3	Total # of cells	0MN	1MN	2MN	3MN	4MN	Total # of MN	MN/500 BN cells	% BN
0	1094	1087	17	0	0	0	17	7.77	61
0.4	471	446	23	2	0	0	27	28.66	49
0.8	541	510	28	3	0	0	34	31.42	55
1.1	446	398	39	7	1	1	60	67.26	52
1.4	290	258	23	6	2	1	45	77.59	47

The kinetics of cells in culture following treatment in suspension with the two radioactive preparations appeared to be different. The radiation-induced reduction (relative to the control) in binucleation for the highest dose (1.4 disintegrations/μm^3) was found to be 30% following 4-[^{123}I]iodoantipyrine treatment and 23% after [^{123}I]NaI exposure. The level of binucleation is a useful parameter to describe how fast cells are growing following irradiation, as cells from both the antipyrine and NaI treatments were cultured for the same time in the same concentration of cytochalasin B. The difference noted is however relatively small and in all cultures useful numbers of binucleated cells could be observed that were suitable for micronuclei counting. Both radioactive preparations were therefore considered appropriate for allowing sufficient cellular kinetics and induction of measurable levels of damage.

The dose response curves for CHO-K1 cells treated with 4-[^{123}I]iodoantipyrine and [^{123}I]NaI are shown in Figure 4.10.

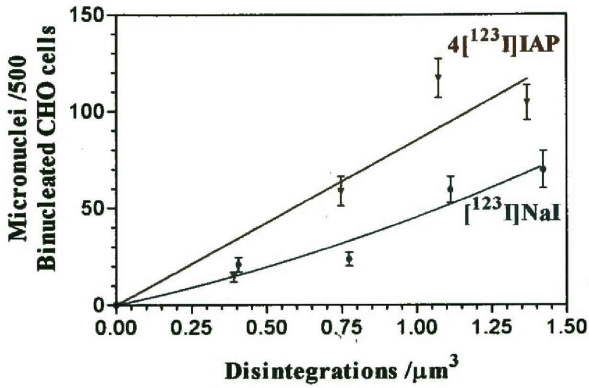

Figure 4.10 Dose response curves representing the number of micronuclei per 500 binucleated CHO-K1 cells as a function of dose after exposure to 4-[^{123}I]iodoantipyrine and [^{123}I]NaI.

Cellular damage was quantified as the number of micronuclei per 500 binucleated cells. It is clear that the different amounts of radioactivity added resulted in different levels of micronuclei formations. The biological damage increased consistently with increasing number of disintegrations per unit volume. Compared to control samples, up to 10 times more micronuclei could be induced with [^{123}I]NaI and 15 times more with 4-[^{123}I]iodoantipyrine. In both cases, the maximum level of micronuclei detected was a result of less than 1.5 disintegrations per μm^3.

The observation that the highest dose of 4-[^{123}I]iodoantipyrine did not translate highest micronuclei yield cannot be due to saturation since the CHO cells have been known to express much higher micronuclei frequencies without an evidence of the dose response reaching a maximum (Slabbert *et al.*, 1999).

Micronuclei frequencies observed in samples irradiated with 4-[^{123}I]iodoantipyrine were significantly higher per number of disintegrations per unit volume than for those treated with [^{123}I]NaI. This is attributed to Auger electrons emitted by ^{123}I in close proximity to cellular DNA, thus contributing to a much higher total biological damage. These findings are supported by the fact that when bacterial cells are exposed to 4-[^{123}I]iodoantipyrine, at least one DNA double strand-break is produced per single decay (Kassis *et al.*, 1999, Hofer *et al.*, 1992). On the other hand, damage from [^{123}I]NaI was considerably lower as the nanometer-ranged Auger electrons emitted outside the cell cytoplasm, are attenuated and do not reach the nuclear DNA. Hence, the damage resulting from [^{123}I]NaI is mainly due to the low-LET 159 keV γ-rays.

A relative biological effectiveness (RBE) of 1.8 was calculated from the data in Figure 4.10. This was defined as the ratio of number of disintegrations from 4-[^{123}I]iodoantipyrine and [^{123}I]NaI required to induce 60 micronuclei per 500 cells. A more elaborative method to estimate the RBE has also been employed. For this, the data in Figure 4.10 were fitted to a second-degree polynomial to estimate the magnitude of the linear and quadratic components of the dose response curves. The equation used is:

$$E = \alpha \cdot Dist + \beta \cdot Dist^2$$

where E is the number of micronuclei per 500 cells and Dist the number of disintegrations per μm^3. α and β are the linear and quadratic coefficients, respectively.

The slope of the dose response data for 4-[^{123}I]IAP treated cells is 85.3 ± 8.9 per disintegration/μm^3 compared to 33.4 ± 16.6 per disintegration/μm^3 for [^{123}I]NaI

treatments. The ratio of these values is 2.6 and reflects the dose limiting RBE observed in this experiment. Although the shape of the dose response curve for [^{123}I]NaI treatments appears to be linear-quadratic, it is in fact no more than a straight line and as such is similar to that of 4-[^{123}I]IAP treated cells. The curvature component for [^{123}I]NaI treated cells was estimated to be 12.1 ± 13.6 per (disintegration μm^3)^2 and was not significantly different from zero. A linear fit yielded a slope of 47.8 ± 3.7 per disintegration μm^3. The steepness of the dose response curve is therefore 1.8 times less than that of 4-[^{123}I]IAP treated cells. This compares to a value of 1.6 observed previously for micronuclei formations in CHO cells treated with the same ^{123}I preparations (Slabbert *et al.*, 1999). Although the ratios of dose response curves are similar, the steepness of both dose response curves is considerably less than that observed by these investigators. The slopes of the dose response curves for the current data sets are less steep by a factor of 4.8 for [^{123}I]NaI treatments and by a factor of 5 for 4-[^{123}I]IAP treated cells. It is concluded that the cells have an increased radioresistance by a factor of about 5. The reasons for this are unclear but may be the result of the CHO-K1 cell line being cultivated over a period of many months. It is also concluded that the marginally larger RBE of 1.8 observed in this work compared to a value of 1.6 reported previously (Slabbert *et al.*, 1999), is the result of the cells being more radioresistant. As a general rule, RBE values increase when cell lines are more resistant to radiation treatment (Slabbert *et al.*, 1996, 2000).

4.4 Irradiation of T-lymphocytes with 4-[^{123}I]iodoantipyrine and [^{123}I]NaI

Human T-lymphocytes were treated with 4-[^{123}I]iodoantipyrine or [^{123}I]NaI as it was believed at the time that lymphocytes were more radioresistant than CHO-K1 cells. For this human lymphocytes were isolated from whole blood samples as described in Chapter 3. The doses of 4-[^{123}I]iodoantipyrine or [^{123}I]NaI are listed in Table 4.16.

Table 4.16 Biological disintegrations of 4-[^{123}I]iodoantipyrine and [^{123}I]NaI in human T-lymphocytes.

	Disintegrations/μm^3	
Volume added (μl)	**4-[^{123}I]IAP**	**[^{123}I]NaI**
0	Control	Control
20	0.481	0.477
40	0.917	0.936
60	1.391	1.378
70	1.606	1.592
80	1.819	1.803

Micronuclei frequencies and the nucleation index (N.I.) observed in these lymphocyte samples are listed in Tables 4.17 and 4.18. The nucleation index is defined as the ratio of total number of nuclei counted in cells to total number of cells analyzed and is a measure of cell proliferation.

Table 4.17 Micronuclei frequency distributions observed in binucleated human T-lymphocytes irradiated with 4-[^{123}I]iodoantipyrine.

Disintegrations/μm^3	Total # of cells	0MN	1MN	2MN	3MN	4MN	5MN	6MN	Total # of MN	MN/500 BN cells	N. I
Control	1649	1586	58	5	0	0	0	0	68	20.62	1.84
0.481	3549	2853	600	81	14	1	0	0	808	113.83	1.92
0.917	2446	1745	570	109	18	3	1	0	859	175.59	1.63
1.391	2627	1083	846	497	150	42	7	2	2505	476.78	1.67
1.606	1616	633	586	282	82	22	10	1	1540	476.49	1.39
1.819	1242	434	352	286	103	42	19	6	1532	616.7	1.71

Table 4.18 Micronuclei frequency distributions observed in binucleated human T-lymphocytes irradiated with [^{123}I]NaI.

Distintegrations/μm^3	Total # of cells	0MN	1MN	2MN	3MN	4MN	5MN	Total # of MN	MN/500 BN cells	N. I
Control	1649	1586	58	5	0	0	0	68	20.62	1.84
0.477	914	781	88	16	3	1	0	133	106.67	1.97
0.936	1438	1173	213	43	8	1	0	327	113.70	1.84
1.378	1750	1350	300	77	17	6	0	529	151.14	1.74
1.592	2801	1892	673	178	45	13	0	1216	217.07	1.72
1.803	2853	1710	777	274	69	18	5	1629	285.49	1.75

To investigate if irradiation with the two preparations affected the nucleation index, the mean indices of the irradiated samples were compared to those in the controls. Subtle changes in the lymphocyte kinetics were observed. The indices were found to be 1.66 and 1.80 for 4-[^{123}I]iodoantipyrine and [^{123}I]NaI, respectively, compared to 1.84 in the controls. The much higher reduction seen in the 4-[^{123}I]iodoantipyrine treated samples

may well be a result of increased mitotic delay due to higher levels of biological damage induced by Auger electrons. In a previous study, an N.I. value of 1.65 was reported for lymphocytes irradiated with 4-[^{123}I]iodoantipyrine (Slabbert *et al.*, 1999). As the stimulation of T-lymphocytes is a very stringent test for cell culture conditions, it may be concluded that the two preparations of ^{123}I used here are indeed biologically friendly in that they do not inhibit the transformation of T-lymphocytes into lymphoblasts.

The micronuclei frequency-dose response curves for lymphocytes are shown in Figure 4.11. The curve corresponding to 4-[^{123}I]iodoantipyrine is much steeper than that for [^{123}I]NaI.

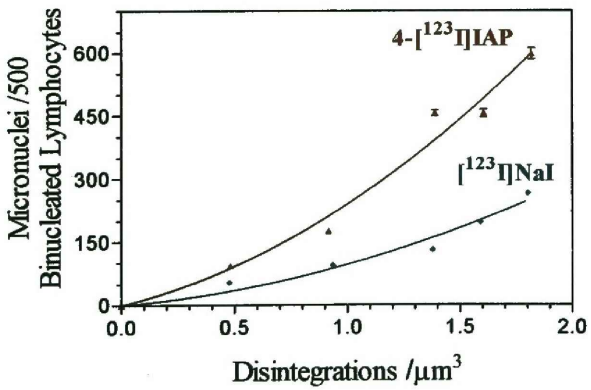

Figure 4.11 Dose response curves representing the number of micronuclei per 500 binucleated lymphocytes as a function of dose after exposure to 4-[^{123}I]iodoantipyrine and [^{123}I]NaI.

Both these dose response curves are very similar to that reported previously by investigators using the same methodology (Slabbert *et al.*, 1999). As in Figure 4.11, the

micronuclei yield per 500 cells for 1.5 disintegrations per μm^3 were reported to be about 150 for lymphocytes treated with ^{123}I labeled to human serum albumin and 500 for 4-[^{123}I]IAP. It is known that human serum albumin, like [^{123}]NaI only allows extracellular disintegration as the cell membrane is impermeable to iodine under normal physiological conditions (Kassis *et al.*, 1980). The small error bars (Figure 4.11) indicate that T-lymphocytes are very reproducible in their response following treatment with these radionuclide preparations.

Fitting the data in Fig. 4.4.1 to the linear-quadratic equation resulted in an α-value of 130.0 ± 67.7 and a β-value of 109.5 ± 42.9 for 4-[^{123}I]IAP treated lymphocytes. Although the standard errors of both parameters are smaller than the mean estimates, the values obtained are somewhat different from expected. The β-value is large relative to the α-estimate and not expected to be significantly different from zero for cells treated with high-LET radiation. The dose response curve for cells treated with [^{123}]NaI has a much lower α-value of 44.9 ± 34.0 and a large β-value of 51.3 ± 21.8. This is consistent with what can be expected for low-LET treatments but again relatively large uncertainties are associated with the estimates. As the quadratic parameters of both response curves are not significant on the 95% confidence level, both data sets can be fitted using linear regression. The ratio of the slopes calculated in this manner is an estimate of the RBE. An RBE of 2.4 was calculated and this was considerably less than the value of 3.7 noted in an earlier study (Slabbert *et al.*, 1999). Even so, a clear expression of Auger electron damage was observed and considerably more micronuclei developed in lymphocytes treated with [^{123}I]IAP.

The objective of this study was to compare the RBE for Auger electrons in cells with different radiosensitivities. Unlike previous investigations, the CHO-K1 cells in this study were more radioresistant than lymphocytes. The RBE value of 2.4 measured for lymphocytes is in fact more than the 1.8 measured for CHO-K1 cells that proved to be very radioresistant. A larger RBE is not anticipated for cells that are more radiosensitive.

It is concluded at this point in the study that the high-LET characteristics of Auger electrons are only reflected in part in the biological data observed this far. RBE values larger than unity are repeatedly noted but they do not change in accordance with expectations based on the different radiosensitivities of the cells used. For this reason it was decided to investigate Auger electron damage using the same cell types but manipulating the radiosensitivity with a radioprotector.

4.5 Irradiation of T-lymphocytes with 4-[^{123}I]iodoantipyrine and [^{123}I]NaI in the presence of a radioprotector β-mercaptoethylamine (MEA)

For this, lymphocytes were isolated from whole blood sample as described in Chapter 3. To 1ml of each cell suspension, 40 μl of 4-[^{123}I]IAP - specific activity 9.5 mCi/ml and 170 μl of [^{123}I] NaI – specific activity 9.85 mCi/ml were added. These activities were chosen to represent different number of disintegrations by the two ^{123}I preparations but these would yield approximately the same level of biological damage.

Just prior to the addition of the radioactivities, the radioprotector β-mercaptoethylamine (MEA) was added to the growth medium to a final concentration of 25 mM. The addition

of MEA to the growth medium however, had two effects. First, a sharp rise in the pH of the growth medium was observed, with the colour of the growth medium changing from pale pink to light purple. Also, test exposures to CHO cells showed that cells lost their distinctive spindle shape and started rounding up in culture. An attempt was made to counteract these changes by adding a few drops of sterile HCl (1 M) to the growth medium. The data for the radioprotector experiments are listed in Table 4.19.

Table 4.19 Micronuclei frequency distributions observed in binucleated human lymphocytes irradiated with 4-[^{123}I]IAP and [^{123}I]NaI in the presence and absence of a radioprotector-MEA.

Disintegrations/μm^3	**Total # of cells**	**0MN**	**1MN**	**2MN**	**3MN**	**Total # of MN**	**MN/500 BN cells**	**N.I**
0.593 4-[^{123}I]IAP	1562	1320	202	35	5	287	91.87	1.59
0.593+MEA 4-[^{123}I]IAP	-	-	-	-	-	-	-	-
2.007 [^{123}I]NaI	1510	1271	209	27	3	272	90.07	1.63
2.007+MEA [^{123}I]NaI	-	-	-	-	-	-	-	-

This experiment was successful only in part as cell samples treated with MEA did not show cytoplasm. It was thought that MEA might be chemically toxic to lymphocytes in 'wet' irradiation. To test this hypothesis, the lymphocytes were irradiated with ^{60}Co γ-rays after being exposed to MEA for 5 and 21 hours. Again, the cells did not maintain their cytoplasm and this seemed to support the idea of chemical toxicity. Another

possibility is that the sudden pH change to a very basic culture environment may have instantly lysed the cells. This can in fact adversely affect the yield of multinucleated cells and micronuclei as shown in Table 4.20. In a previous study, when MEA was added to whole blood before irradiation and lymphocyte isolation, normal cytoplasm and cellular kinetics were observed (Ntuane 2000). This is evidence that MEA is not chemically toxic to lymphocytes.

Table 4.20 Cell kinetics observed on human T-lymphocytes irradiated with ^{60}Co in the presence or absence of MEA.

Dose	Cells with N number of nuclei				Number of MN observed		RESULTS
	1 MN	2 MN	3 MN	4 MN	1 MN	2 MN	
Control	845	1209	153	67	401	249	Normal kinetics
5 Gy, No MEA	599	901	87	31	183	72	Normal kinetics
0 Gy, MEA, 5 hours	15	42	-	-	3	-	Shortage of cells. Less binucleation. Most cells undivided. Lack of c o lasm
5 Gy, MEA, 5 hours	6	11 Lack of c o lasm	-	-	-	-	Few binucleated cells. The rest lack cytoplasm
0 Gy, MEA, 21 hours	39	13 Lack of cytoplasm	-	-	1	-	Few cells stimulated; binucleated & trinucleated cells can be seen but mostly with no cytoplasm. Ma'orit did not divide.
5 Gy, MEA, 21 hours	21	04 Lack of cytoplasm	-	-	-	-	No shortage of cells but less stimulation; binucleation can be observed mostly in cells with no c o lasm

4.6 Irradiation of CHO-K1 clone #16 cells with 4-[^{123}I]iodoantipyrine and [^{123}I]NaI in the presence of a radioprotector β-mercaptoethylamine (MEA)

To establish whether the effects of MEA (in combination with the radioactive preparations) seen in lymphocytes are also present when cell types that are already in a state of growth and do not require stimulation into mitosis, we repeated the above experiment using CHO-K1 #16 cells. For this, the cells were irradiated with 4-[^{123}I]iodoantipyrine and [^{123}I]NaI in the presence of a radioprotector-MEA. The doses of 4-[^{123}I]iodoantipyrine or [^{123}I]NaI in CHO-K1 #16 cell suspensions with and without the radioprotector are listed in Table 4.21.

Table 4.21 Disintegrations of 4-[^{123}I]iodoantipyrine and [^{123}I]NaI per unit volume in CHO-K1 #16 cells in the presence and absence of the radioprotector.

4-[^{123}I]IAP		[^{123}I]NaI	
Volume added (μl)	**Disintegrations per μm^3**	**Volume added (μl)**	**Disintegrations per μm^3**
Control	0.00	Control	0.00
60	0.775	110	1.420
60+MEA	0.775+ MEA	110+MEA	1.420+ MEA

Cellular damage was quantified from micronuclei that formed in binucleated cells and the data presented in Table 4.22.

Table 4.22 Micronuclei frequency distributions observed in CHO-K1 #16 cells irradiated with 4-[^{123}I]IAP and [^{123}I]NaI in the presence and absence of a radioprotector-MEA .

integrations	Total # of cells	0MN	1MN	2MN	3MN	4MN	Total # of MN	MN/500 BN cells	% BN
1 Control	2681	2662	17	2	0	0	21	3.92	78.33
ntrol+MEA	564	552	11	1	0	0	13	11.52	38.5
75 4-[^{123}I]IAP	3802	2780	869	135	13	4	1192	156.76	70.6
75 4-[^{123}I]IAP+MEA	428	376	46	5	1	0	59	68.92	26.76
2 [^{123}I]NaI	2814	2169	579	63	3	0	714	126.87	71.14
12 [^{123}I]NaI + MEA	979	866	97	13	03	0	132	67.42	28.37

The proportion of cells that were binucleated dropped from about 70 and 80% in control samples to between 26 and 38% in unirradiated samples treated with MEA. This indicates that cellular kinetics were again severely disturbed and further supports the idea that the drastic changes in pH in normal culture media upon addition of MEA do have an influence on the experimental outcome. All cells however, retained their cytoplasm and micronuclei counts could therefore be made as illustrated in Figure 4.12. The attachment of the CHO cells may have slowed down the pH-induced lysis process, and hence the observation that the cytoplasma were intact. The low proliferation may be attributed a high proportion of cells being inactivated by the increased pH.

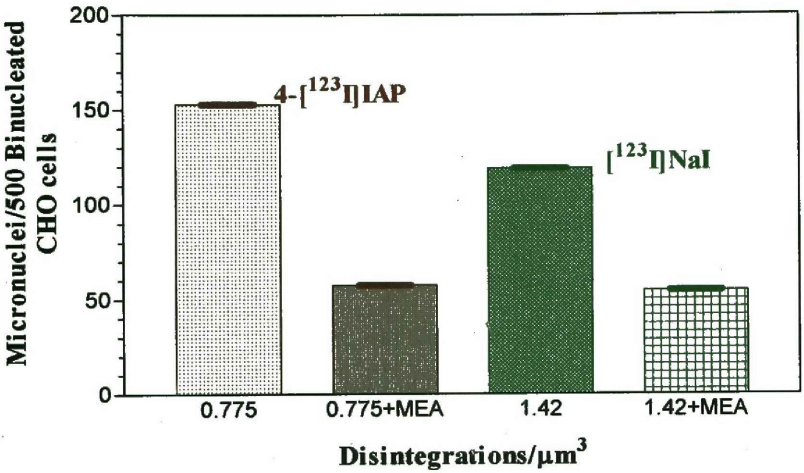

Figure 4.12 Micronuclei frequencies and radioprotection observed in CHO-K1 cells irradiated with 4-[^{123}I]IAP and [^{123}I]NaI in the absence and presence of MEA.

The bar chart in Figure 4.12 shows the protective effect of MEA on cells irradiated with low-LET radiation ([^{123}I]NaI) and high-LET radiation (4-[^{123}I]iodoantipyrine). Since Auger electrons are high-LET in nature, it was expected that the protection efficiency of MEA will be relatively high with [^{123}I]NaI and less or even negligible with 4-[^{123}I]iodoantipyrine (high-LET). Interestingly, a striking level of protection was observed for the [^{123}I]IAP treated cells. MEA treatment resulted in 56 and 47% reduction in micronuclei yield in 4-[^{123}I]iodoantipyrine and [^{123}I]NaI treated cultures, respectively. The higher protection from 4-[^{123}I]iodoantipyrine damage may be due to the fact that MEA, a primary radical scavenger, is capable of protecting cells from Auger electron damage which is mostly indirect. Similarly, it can be expected that MEA is not as efficient in protecting against the direct damage due to the low-LET gammas from

[^{123}I]NaI. In contrast, CHO-K1 cells irradiated in the presence of MEA with [^{125}I]iododeoxyuridine showed a differential protective effect for low-LET and high-LET radiation configurations (Hofer & Bao 1995). These investigators irradiated cells in the frozen state following exposure to ^{125}I-deoxyuridine for different times. Cells exposed to this formulation for only 30 minutes reflected typical low-LET radiation damage and substantial protection by MEA could be demonstrated. However, a 5-hour exposure showed high-LET radiation damage and for this little protection was achieved by the addition of MEA. The differences between these findings and our observation may be explained by the differences in experimental set-up.

The protective efficiency of MEA at concentration of 1.3 mM in Chinese hamster V79 lung fibroblasts treated with ^{210}Po-citrate, ^{125}IdU and ^{131}IdU has been assessed (Biyashee *et al.*, 2000). Although the lethal effects of DNA incorporated ^{125}IdU have been reported to be similar to those caused by 5.3 MeV α-particles emitted by ^{210}Po (Howell *et al.*, 1998), the protective effect of MEA was observed to be substantially higher for Auger electrons than α-particles. Dose-modifying values of 1.4, 1.7 and 1.8 were obtained for ^{210}Po-citrate, ^{125}IdU and ^{131}IdU treated samples, respectively. Comparing these investigations with our work, it can be concluded that the mode in which Auger electrons cause damage is not the same as for α-particles. Therefore, Auger electrons are not strictly high-LET radiation and the biological nature of radionuclides that emit Auger electrons are very dependent on exactly where in the cell the isotope disintegrates.

Having not been successful in demonstrating a differential yield in micronuclei in the MEA treated 4-[^{123}I]IAP and [^{123}I]NaI samples, it was decided to do the experiment again using cells that are very radiosensitive.

4.7 Radiosensitivity tests with ^{60}Co γ-rays

Test exposures were performed on three different cell lines namely CHO-K1 #7, CHO-K1 #16 and CHO-XRS 1 to evaluate their inherent radiosensitivities. Previous studies have demonstrated that the surviving fraction at 2 Gy for CHO-K1 #7, CHO-K1 #16 and CHO-XRS 1 were 0.51, 0.56 and 0.06, respectively (Sebeela 2000). In the current investigation, the cells were irradiated with 2 Gy of ^{60}Co γ-rays and the resulting damage from micronuclei formation enumerated and used as a measure of radiosensitivity (Table 4.23).

Table 4.23 Micronuclei frequency distributions observed in CHO-K1 #7, CHO-K1 #16 and CHO-XRS 1 cells irradiated with 2 Gy of ^{60}Co γ-rays.

Cell line	Dose (Gy)	BN	1MN	2MN	3MN	4MN	Total # of cells	Total # of MN	MN/500 BN cells
CHO-K1 #7	2	516	171	49	11	3	750	314	209.33
CHO-K1 #16	2	503	112	15	3	1	634	155	122.24
CHO-XRS 1	2	103	75	39	8	8	233	209	448.50

The results obtained showed that CHO-XRS 1 cells were more radiosensitive than the rest, with CHO-K1 #16 clone being the most resistant type and about twice as radioresistant than CHO-K1 # 7 clone (Figure 4.13). These data are consistent with radiosensitivity measured by colony formation (Sebeela 2003)

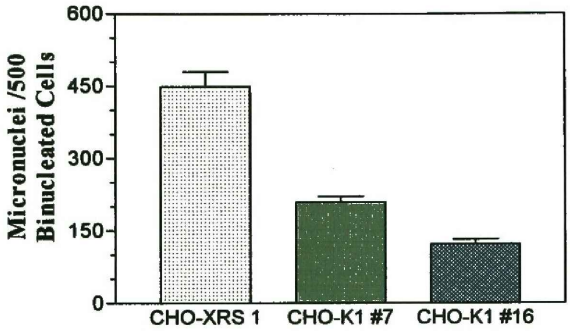

Figure 4.13 Micronuclei frequency observed in CHO-K1 #7, CHO-K1 #16 and CHO-XRS 1 cells irradiated with 2 Gy of ^{60}Co γ-rays.

Clearly, the CHO-XRS 1 cell line was most radiosensitive compared to the CHO-K1 #16 cells used in previous experiments. For this reason, the CHO-XRS 1 cells were exposed to 4-[^{123}I]IAP and [^{123}I]NaI.

4.8 Irradiations of CHO-XRS 1 cells with 4-[^{123}I]iodoantipyrine and [^{123}I]NaI

The number of ^{123}I disintegrations per unit volume generated in the cell suspensions are listed in Table 4.24. Control samples were not exposed to radiation.

Table 4.24 Activities used and number of disintegrations of 4-[^{123}I]iodoantipyrine and [^{123}I]NaI in CHO-XRS cells.

4-[^{123}I]IAP		[^{123}I]NaI	
Volume added (μl)	**Disintegrations per μm^3**	**Volume added (μl)**	**Disintegrations per μm^3**
Control	0.00	Control	0.00
30	0.399	40	0.546
60	0.775	80	1.052
100	1.245	120	1.522
130	1.576	160	1.959

Unlike CHO-K1 cells, CHO-XRS 1 cells took about 48 hours to show a substantial level of binucleation. Cellular damage quantified as micronuclei in binucleated cells and apoptotic bodies are shown in the Tables 4.25 and 4.26.

Table 4.25 Micronuclei frequency distributions observed in CHO-XRS 1 cells irradiated with 4-[^{123}I]IAP.

tegra-ns /μm^3	**Total # of cells**	**0MN**	**1MN**	**2MN**	**3MN**	**4MN**	**Total # of MN**	**MN/500 BN cells**	**% BN**	**No. of apoptotic bodies/500 cells**
1	832	814	18	0	0	0	18	10.82	47.01	0
	646	460	151	29	5	1	228	176.47	36.21	19
75	304	226	52	22	3	1	109	179.28	34.35	52
5	508	388	77	26	12	5	185	182.09	31.0	71
4	786	675	74	25	11	1	161	102.42	25.1	92

Table 4.26 Micronuclei frequency distributions observed in CHO-XRS 1 cells irradiated with [^{123}I]NaI.

Disintegrations /μm^3	Total # of cells	0MN	1MN	2MN	3MN	4MN	Total # of MN	MN/500 BN cells	% BN	No. of apoptotic bodies / 500 cells
Control	832	814	18	0	0	0	18	10.82	47.01	0
0.546	1252	770	347	122	13	0	630	251.59	39.86	0
1.052	878	538	227	90	17	5	481	273.92	35.22	5
1.522	819	589	151	61	15	3	330	201.47	32.68	16
1.959	771	598	115	34	18	6	261	169.26	22.31	46

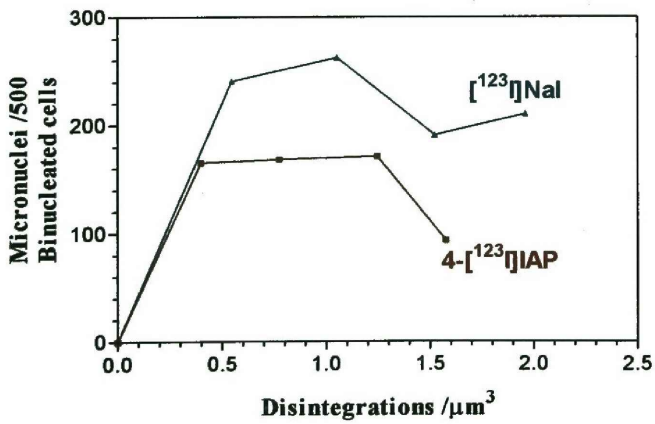

Figure 4.14 Micronuclei frequencies showing biological damage in CHO-XRS 1 cells irradiated with 4-[^{123}I]Iodoantipyrine and [^{123}I]NaI.

CHO-XRS cells turned out to be extremely sensitive to the ^{123}I treatments. Micronuclei frequencies in all samples started very high for doses as low as 0.5 disintegrations/μm^3 and remained about the same for samples exposed to higher levels of radioactivity (Figure 4.13). Notwithstanding the fact that reasonable levels of binucleation were observed, a clear saturation in micronuclei yield was evident at 1.0 disintegrations/μm^3 and above. A striking observation in these samples was the extensive levels of apoptosis. Apoptosis appeared to increase with radioactivity and was much higher in the 4-[^{123}I]IAP samples. This may be the reason for the lower average micronuclei yield in samples affected by Auger electrons. It was concluded that the very radiosensitive CHO-XRS 1 cells were not suitable to study Auger electron damage using micronuclei as an endpoint. For this reason CHO-K1 cells, clone #7 that was also identified to be relatively radiosensitive were similarly assessed.

4.9 Irradiation of CHO-K1 clone #7 cells with 4-[^{123}I]iodoantipyrine and [^{123}I]NaI

The data for disintegrations of 4-[^{123}I]IAP and [^{123}I]NaI in CHO-K1 #7 cell cultures are listed in Table 4.27.

Table 4.27 Disintegrations of 4-[^{123}I]iodoantipyrine and [^{123}I]NaI in 1 ml CHO-K1 #7 cell suspensions.

4-[^{123}I]IAP		[^{123}I]NaI	
Volume added (μl)	**Disintegrations per μm^3**	**Volume added (μl)**	**Disintegrations per μm^3**
40	0.41	50	0.50
60	0.60	90	0.86
80	0.78	130	1.20
100	0.96	170	1.52
130	1.21	-	-

Following exposure of the CHO-K1 #7 cells to the doses of 4-[^{123}I]IAP and [^{123}I]NaI, the resulting micronuclei yield are presented in Tables 4.28 and 4.29

Table 4.28 Micronuclei frequency distributions observed in CHO-K1 #7 cells irradiated with 4-[^{123}I]iodoantipyrine.

Disinte-grations/μm^3	**Total # of cells**	**0MN**	**1MN**	**2MN**	**3MN**	**4MN**	**5MN**	**Total # of MN**	**MN/500 BN cells**	**% BN**
Control	3732	3688	38	6	-	-	-	50	6.70	81.75
0.41	3183	2672	462	92	3	-	-	563	88.44	73.15
0.60	3581	2760	714	92	13	2	-	945	131.95	82.19
0.78	4124	2951	959	193	15	5	1	1415	171.56	83.31
0.96	4150	2724	1132	245	34	11	4	1788	215.42	83.07
1.21	4412	2531	1436	356	64	21	4	2444	276.97	77.93

Table 4.29 Micronuclei frequency distributions observed in CHO-K1 #7 cells irradiated with [^{123}I]NaI.

Disinte-grations/μm^3	Total # of cells	0MN	1MN	2MN	3MN	4MN	5MN	Total # of MN	MN/500 BN cells	% BN
Control	3732	3688	38	6	0	0	0	50	6.70	81.75
0.41	4161	3689	438	34	0	0	0	506	60.80	79.97
0.60	4472	5390	778	95	9	0	0	995	111.25	80.66
0.78	4566	3504	939	107	15	1	0	1202	131.63	80.45
0.96	5305	3726	1331	205	30	11	2	1885	177.66	77.06

A large number of cells were examined in this run. In this data set, it was clear that cellular kinetics following treatment were normal for cells exposed to both ^{123}I preparations. As high as 80% binucleation could be obtained for cells treated with both 4-[^{123}I]IAP and [^{123}I]NaI, and cellular kinetics appeared to be unchanged compared to controls.

The relationship between micronuclei yield and dose of 4-[^{123}I]IAP and [^{123}I]NaI was linear (Figure 4.14). The slopes of the dose response curves for the two preparations were however very different, indicating that Auger electron damage was evident. Also, a substantial increase in radiosensitivity was noted in clone #7 compared to CHO-K1 #16 cells. The ratio of slopes for clone #7 to clone #16 for 4-[^{123}I]IAP or [^{123}I]NaI treatment was 2.5.

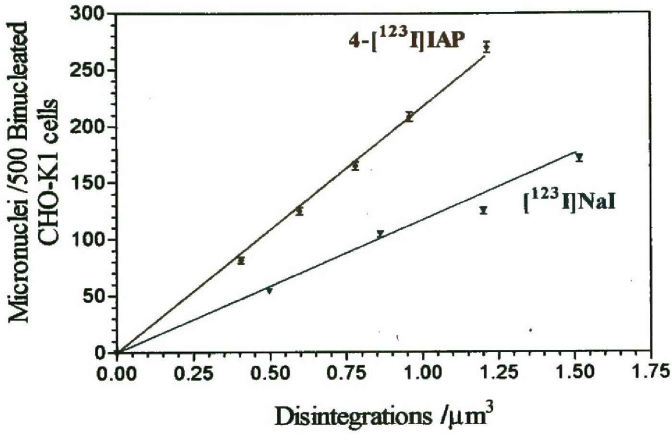

Figure 4.15 Dose response curves representing the relationship between micronuclei frequencies per 500 binucleated CHO-K1 #7 cells irradiated with 4-[^{123}I]IAP and [^{123}I]NaI and the number of disintegrations per unit volume.

As observed with CHO-K1 #16 cells and lymphocytes, more biological damage was observed in CHO-K1 #7 cells irradiated with 4-[^{123}I]IAP than in those treated with [^{123}I]NaI. However, for a given number of disintegrations clone #7 exhibited a much higher micronuclei yield than clone #16. From 4.14, about 170 micronuclei per 500 binucleated cells correspond to 0.80 disintegrations per cubic micrometer for 4-[^{123}I]IAP treated cells. In cell samples treated with [^{123}I]NaI, about 1.50 disintegrations/μm^3 were needed to produce the same biological effect. This corresponds to an RBE value of 1.9 that compares well with the value of 1.8 noted for clone #16.

Fitting the data in Figure 4.14 to a linear-quadratic equation, the dose response curve parameters for 4-[^{123}I]IAP treated cells resulted in an α-value of 193.8 $\pm$ 2.0 and a β-

value of 24.1 ± 2.0. For both coefficients, the standard error is much smaller than the estimate and a small but significant quadratic component was therefore noted. A straight-line fit of this data resulted in a slope of 217.2 ± 2.7. For cells treated with [^{123}I]NaI the β-value was negative but not significantly different than zero. For this reason the data were fitted to a straight line to give a slope of 117.3 ± 3.2. The ratio of the slopes yielded an RBE value of 1.9 and this is consistent with that calculated using the ratios of number of disintegrations required to induce the same level of micronuclei (Figure 4.14). It would appear therefore that even with a substantial increase in radiosensitivity by as much as 2.5 times compared to the radioresistant clone #16, the RBE remains unchanged.

4.10 Summary of irradiation results

The results obtained from this work indicate that micronuclei frequencies induced by 4-[^{123}I]IAP are consistently higher than those induced by [^{123}I]NaI. This supports the notion that the cytotoxic effects of Auger electrons are due to the intracellular disintegration of the 4-[^{123}I]IAP formulation, and that disintegration of [^{123}I]NaI is limited to the outside of the cytoplasm.

As the relative response (RBE) of cells treated with the two formulations is of prime interest in this study, data obtained were compared to that of other investigators using the ratio of slopes 4-[^{123}I]IAP to [^{123}I]NaI as a function of radiosensitivity. For this purpose, radiosensitivity was defined as micronuclei frequency per unit disintegration of the reference radiation ([^{123}I]NaI). RBE values ranging between 1.6 and 3.7 are listed in Table 4.30.

Table 4.30 The slopes of dose responses expressed as micronuclei frequency per 500 binucleated cells/disintegrations /μm^3 for 4-[^{123}I]IAP and [^{123}I]NaI (B/A) in various cells lines. A and B are the slopes for [^{123}I]NaI and 4-[^{123}I]IAP treatments, respectively. r is the regression coefficient.

Cell line	[^{123}I]NaI (A)	R^2	4-[^{123}I]IAP (B)	r^2	B/A
A549 (Smit *et al.*, 2001)	43±7	0.819	134 ± 10	0.939	3.1
ATs4 (Smit *et al.*, 2001)	69±13	0.634	123±9	0.936	1.8
CHO (Smit *et al.*, 2001)	213±11	0.938	334±17	0.933	1.6
DMBA (Smit *et al.*, 2001)	293±23	0.719	527±32	0.933	1.8
Nortje (Smit *et al.*, 2001)	239±18	0.941	698±9	0.998	2.9
AT (Smit *et al.*, 2001)	432±23	0.948	948±90	0.764	2.2
CHO-K1#7 (This work, 2004)	117 ± 3	0.989	217 ± 3	0.997	1.9
CHO-K1#16 (This work, 2004)	47 ± 4	0.933	85± 9	0.891	1.8
Lymphocytes (This work, 2004)	123 ± 9	0.916	299 ± 20	0.939	2.4
CHO-K1 (Slabbert *et al.*, 1999)	239 ± 26	-	410 ± 34	-	1.6
Lymphocytes (Slabbert *et al.*, 1999)	93 ± 12	-	341 ± 22	-	3.7

Having the results of 11 cell lines all exposed to both 4-[^{123}I]IAP and [^{123}I]NaI it was of interest to assess the relationship between RBE and radiosensitivity as shown in Figure 4.15.

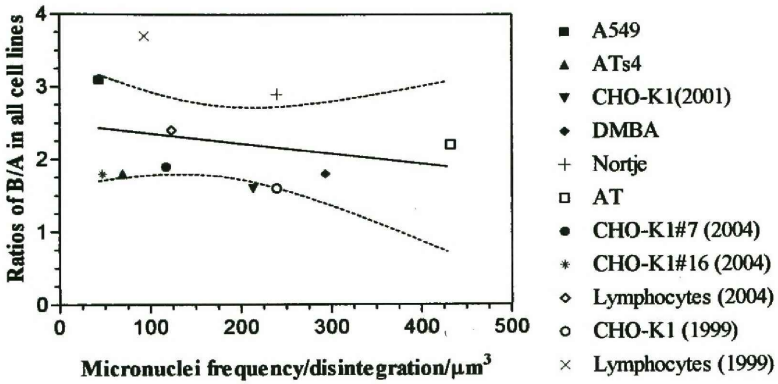

Figure 4.16 The ratios of the slopes of micronuclei-dose response curves for 4-[^{123}I]IAP (B) and [^{123}I]NaI (A) exposure in eleven cells lines as a function of radiosensitivity expressed as micronuclei frequency/disintegration/μm^3 with [^{123}I]NaI exposures.

Linear regression analysis of the data in Table 4.30 yielded a slope of –0.0014 ± 0.0019. As the standard error is higher than the actual estimate, the slope of the line is therefore statistically insignificant. On average, the slope is negative suggesting a small decrease in RBE with increasing radiosensitivity. This observation is consistent with that seen when cell types of various radiosensitivities were treated with neutrons and RBE values were compared to their radiosenstivity following irradiation with ^{60}Co γ-rays or high energy X-rays (Theron *et al.*, 1997, Slabbert *et al.*, 2000).

CHAPTER V

5. Conclusions and Recommendations

5.1 Conclusions

In this work, 4-iodoantipyrine was synthesized from antipyrine (phenazone) using NaI and chloramine-T as an oxidizing agent. HPLC analyses showed that at least 5 re-crystallizations in ethanol were required to purify the product. Following this, a stable product was then available for ion exchange reactions.

The radioiodination of 4-iodoantipyrine can, in principle, be effected using a variety of methods. These include silica surface catalyzed iodination, the use of chloramine-T as an oxidant, isotope exchange by the melt technique and radioisotopic exchange with 4-bromoantipyrine. A method using the phosphate buffer $NaHPO_4$ and NaOH was selected for routine use in this work and proved to be most efficient as eluate fractions with labeling efficiencies of more than 95% could be obtained. Also, reasonable consistency in the specific activity of the labeled compound was noted. As such, a pure compound with a high specific radioactivity was produced that allowed the study of Auger electron damage in a variety of cell types, as the compound induced measurable levels of micronuclei yield. Furthermore, when added to cells in culture 4-[^{123}I]iodoantipyrine resulted in much higher levels of biological damage compared to that caused by the same levels of disintegrations from [^{123}I]NaI. This indicated that sufficiently high radioactive concentrations may be used to induce high levels of biological damage without interfering with the kinetics of cells in culture.

The short lived ^{123}I was used in this study since it allows cells to be irradiated without the need to freeze samples in liquid nitrogen for long periods as suggested by other investigators (Walicka, *et al.*, 2001, Hofer and Bao, 1995). The advantage of this is clearly illustrated by the significant differences in the level of biological responses observed when cells were irradiated with ^{60}Co γ-rays at room temperature (37°C) and in frozen state (–196°C). From these results, higher micronuclei frequencies were observed in cultures irradiated at room temperature than in frozen state. On the contrary, the percentage binucleation for cells irradiated in frozen state was higher compared to cells treated at room temperature, possibly indicating an extended mitotic delay of the latter samples due to more radiation damage. This suggests that biological effects of Auger electrons may be studied more efficiently at normal physiological conditions than in frozen state. The high protection observed in cells irradiated in the presence of a chemical protector MEA, with 4-[^{123}I]iodoantipyrine than with [^{123}I]NaI, shows that Auger damage is not strictly high-LET. Hence in targeted therapy, the efficiency of Auger electrons can be expected to change with tumour radiosensitivity.

The consistency in the results obtained in this study and those from previous studies (Slabbert *et al.*, 1999, Smit *et al.*, 2001) shows that mammalian cell response to Auger electron damage can be clearly demonstrated. Lymphocytes were found to be more resistant (RBE = 2.4) than the CHO cells lines. However, the RBEs obtained for the CHO-K1 clones #16 and clone #7 were 1.8 and 1.9, respectively, and did not reflect the differences in radiosensitivity as determined by colony formation. It is possible that RBE calculated from MN yield cannot detect the inter-cell line differences in radiosensitivity

usually observed in conventional assays. Also, the high low-LET component in both the test and reference radiations may have overshadowed minor differences due to the Auger electrons. The incomplete data obtained from CHO-XRS 1 cells shows that this cell line is extremely sensitive and may not be suitable for Auger electron studies.

5.2 Recommendations

Since antipyrine does not bind to cellular DNA, it is likely that the damage due to Auger electrons is considerably moderated. It is therefore, possible that by using radionuclide carriers that specifically bind to the DNA may result in much higher Auger electron doses and elevated biological damage. In this regard, deoxyuridine which is also a radiosensitizer is recommended for further studies on cellular responses to Auger electron damage.

REFERENCES

Akudugu, J. M., Theron, T., Serafin, A. M. and Böhm, L. (2004). Influence of DNA double-strand break rejoining on clonogenic survival and micronucleus yield in human cell lines. *Int. Journ. Radiat. Biol.* **80** (2) : 93-104.

Barendsen, G. W. and Walter, H. M. D. (1964). Effects of ionizing radiations on human cells in tissue culture. *Radiat. Res.* **21** : 314-329.

Behr, T. M., Behe, M., Lohr, M., Sgouros, G., Angerstein, C., Wehrmann, E., Nebedahl, K., and Becker, W. (2000). Therapeutic advantage of Auger electron –over β-emitting radiometals or radioiodine when conjugated to internalizing antibodies. *Euro. Journ. Nuc. Med.* **27**: 753-765.

Behr, T. M., Sgouros, G., Vougiokas, V., Memtsoudis, S., Gratz, S., Schmidebrger, H., Blumenthal, R. D., Goldberg. D. M. and Becker, W. (1998). Therapeutic efficacy and dose-limiting toxicity of Auger-electron vs. beta emitters in radioimmunotherapy with internalizing antibodies: evaluation of ^{125}I- vs. ^{131}I-labeled CO17-1A in a human colorectal cancer model. *Int. Journ. Cancer.* **76** (5): 738-748.

Bernhardt, P. and Forssell-Aronsson, E. (2001) Electron emitting radionuclides for targeted therapy. Dept of Radiation physics, Geteborg University, Shlgrenska University Hospital, SE-413 45 Goteborg, Sweden.

Bethge, W. A. and Sandmaier, B. M. (2004). Targeted cancer therapy and immunosuppression using radiolabeled monoclonal antibodies. *Semin. Oncol.* **31** (1): 68-82.

Bird, R. P. (1980). Cysteamine as a protective agent with high-LET radiations. *Radiat. Res.* **82**: 290-296.

Bishayee, A., Rao, D. A. and Howell R. W. (2000). Radiation protection by cysteamine against the lethal effects of intracellularly localized Auger electron, α- and β- particle emitting radionuclides. *Acta Oncol.* **39** (6): 713-720.

Bodei, L., Kassis, A. I., Adelstein, S. J. and Mariani, G. (2003). Radionuclide therapy with Iodine-125 and other Auger-electron-emitting radionuclides: experimental modes and clinical applications. *Cancer Biother. Radiopharm.* **18** (6): 861-877.

Chen, P. Cameron, R. Wang, J. Vallies, K. A. and Reilly, R. M. (2003). Anti-tumour effects and normal tissue toxicity of ^{111}In-labeled epithermal growth factor administered to mice bearing epidermal growth factor receptor-positive human breast cancer xenografts. *Jour. Nuc. Med.* **44** (9): 1469-1478.

Dietze, G. (1999). Environmental and occupational dosimetry: An integrated approach to radiation protection covering radioecology dosimetry and biological effects. Summary of the work of the action group of EULEP.

Digvi, C. H. (2002). Radioimmunotherapy in solid and hematologic neoplasms. Cancer research institute. Memorial Sloan-Kettering cancer center, New York.

Feinendegen, L. E. (1991). Contributions of nuclear medicine to the therapy of malignant tumours. *Strahlenther. Oncol*: **167** (11): 619-627.

Goddu, S. M., Howell, R. W. and Rao, D. V. (1994). Cellular Dosimetry: absorbed fractions for monoenergetic electron and alpha particle sources and S-values for radionuclides uniformly distributed in different cell compartments. *Journ. Nucl. Med.* **35**: 303-316.

Govindan, S. V., Goldenberg, D. M., Elsamra. S. E., Griffiths, G. L., Ong, G. L., Brechbiel, M. W., Burton, J., Sgouros, G. and Mattes, M. J. (2000). *Journ. Nucl. Med.* **41** (12) : 2089-2097.

Grachev, S. A. and Sverdlov, A. G. (1997). Chemical protection against X-ray, gamma, and neutron radiation. Armed Forces Radiobiology Research Institute (AFRRI) Contract report 97-1, Defense Nuclear Agency Contract DNA001-93-C-0155. Gatchina, Russia.

Gragg, R. L., Humphrey, R. M., Thomas, H. D. Jr. and Meyn, R. E. (1978). The response of Chinese hamster ovary cells to fast neutron radiotherapy beams. *Radiat. Res.* **76** : 283-291.

Hall, E. J. 4th edition. (1998). Radiobiology for the radiologist. Lippincott Williams & Wilkins, USA.

Hall, E. J. 5th edition. (2000). Radiobiology for the radiologist. Lippincott, Williams & Wilkins, USA.

Hofer, K. G. and Bao, S. (1995). Low-LET and high-LET radiation action of ^{125}I decays in DNA: effect of cysteamine on micronucleus formation and cell killing. *Radiat. Res.* **141**: 183-192.

Hofer, K. G. (2000). Biophysical aspects of Auger processes. *Acta. Oncol.* **39** (6): 651-657.

Hofer, K.G., van Loon, N., Schneiderman, M. H. and Charlton, D. E. (1992). The paradoxical nature of DNA damage and cell death induced by ^{125}I decay. *Radiat. Res.* **130** :121-124.

Howell, R. W. (1992). Radiation spectra for Auger-electron emitting radionuclides: Report No.2 of AAMP nuclear medicine task group No. 6[a)].

Howell, R. W., Goddu, S. M., Biyashee, A. and Rao, D. A. (1998). Radioprotection against lethal damage caused by chronic irradiation with radionuclides *in vitro*. *Radiat. Res.* **150**: 391-399.

Humm, J. L. and Charlton, D. E. (1989). A new calculation method to assess the therapeutic potential of Auger electron emission. *Int. J. Radiation Oncology. Biol. Phys.* **17** : 351-360.

Humm, J. L. (1987). Microdosimetric model of astatine-211 labeled antibodies for radioimmunotherapy. *Int. Journ. Oncol. Biol. Phys.* **13** : 11-18.

Humm, J. L., Howell, R. W. and Rao, D. V. (1994). Dosimetry of Auger-electron-emitting radionuclides: report no. 3 of AAPM nuclear medicine task group no. 6[a)]. *Med. Phys.* **21** (12): 1901-1913.

Karagiannis, T. (2003) Consideration of molecular damage induced by auger electron emitting isotopes using 125I as an example. *Hell. J. Nucl. Med.* **6** (3): 138-143.

Karamychev, V. N., Zhurkin, V. B., Garges, S., Nuemann, R. D., and Panyutin, I. G. (1999). Detecting the DNA links in a DNA-CRP complex in solution with Iodine-125 radioprobing.doc: 10.1038/11519. 6 : 747-750.

Kassis, A. I. and Adelstein, S. J. (1980). A rapid and reproducible method for the separation of cells from radioactive media. *Journ. Nucl. Med.* **21**: 88-90.

Kassis, A. I., Harapanhalli, R. S. and Adelstein, S. J. (1999). Comparison of strand breaks in plasmid DNA after positional changes of Auger electron emitting Iodine-125. *Radiat. Res.* **151** : 167-176.

Kassis, A. I., Sastry, K. S. R. and Adelstein, S. J. (1987). Kinetics of uptake, retention, and radiotoxicity of ^{125}IudR in mammalian cells: implications of localized energy deposition by Auger processes. *Radiat. Res.* **109** : 78-89.

Kearney, T., Hughes, A., Hanson, R. N. and DeSombre, E. R. (1999). Radiotoxicity of Auger electron-emitting estrogens in MCF-7 spheroids: A potential treatment for estrogen receptor-positive tumours. *Radiat. Res.* **151** : 570-579.

Köksal, G., Dalcí, D. Ö. and Pala, F. S. (1995). Micronuclei in human lymphocytes: the ^{60}Co gamma-ray dose-response. *Mutat. Res.* **359** : 151-157.

Lamki, L. M. (2000). Therapy with radionuclides: clinical acceptance is overdue. *Medic. Sci.* **2** : 69-73.

le Roux, J., Slabbert, J., Smit, B. and Blekkenhorst, G. (1998). Assessment of the micronucleus assay as a biological dosimeter using cytokinesis-blocker lymphocytes from cancer patients receiving fractionated partial body–radiotherapy. *Strahlenther. Onkol.* **174** (2) : 72-81.

Maschauer, S., Prante, O., Hoffmann, M., Diechen, J. T. and Kuwert, T. (2004). Characterization of ^{18}F-FDG uptake in human endothelial cells *in vitro*. *Journ. Nucl. Med.* **45**: 455-460.

Michel, R. B., Brechbiel, M. W. and Mattes, M. J. (2003). A comparison of 4 radionuclides conjugated to antibodies for single-cell kill. *Journ. Nucl. Med.* **44** (4) : 632-640.

Miyazaki, N. and Shinohara, K. (1993). Cell killing induced by decay of ^{125}I during the cell cycle: Comparison of ^{125}I-Antipyrine with ^{125}I-Bovine serum bovine albumin. *Radiat. Res.* **133**. 182-186.

Nakamura, J., Shaw, C. M. and Brown, D. Q. (1987). Hydrolysis of WR-2721 by mouse liver fractions. *Radiat. Res.* **109**: 143-152.

Narra, V. R., Howell, R. W., Harapanhalli, R. S., Sastry, K. S. and Rao, D. V. (1992). Radiotoxicity of some iodine-123, iodine-125, and iodine-131-labeled compounds in mouse testes: implications for radiopharmaceutical design. *Journ. Nucl. Med.* **33** (12): 2196-2201.

Neumann, R. D., Panyutin, I., Karamychev, V., Sedelnikova, A., Winters, A. T., V., Mezhevaya, K. and Voloshin, Y. (1999). Intramural research project Z01 Cl-60001-04 NMRR: Gene-specific radiotherapy. Annual report.

Ntuane, B. L. (2000). The effectiveness of Cysteamine as a radioprotector against cellular damage induced by fast neutrons. MSc thesis: UNW, iThemba LABS.

O'Donoghuel, J. A. and Wheldon T. E. (1996) Targeted radiotherapy using Auger electron emitters. *Phys. Med. Biol.* **41**: 1973-1992.

Ochakovskaya, R., Osorio, L., Goldenberg, D. M. and Mattes, J. M. (2001). Therapy of disseminated B-Cell lymphoma xenografts in severe combined immunodeficient mice with an anti-CD74 antibody conjugated with ^{111}Indium, ^{67}Gallium, ^{90}Yttrium. *Clin. Canc. Res.* **7**: 1505-1510.

Qaim, S. M. (2001) Therapeutic radionuclides and nuclear data. *Radiochim. Acta* **89**: 297-302.

Rao, V. R., Narra, V. R., Howell, R. W., Lanka, V. K. and Sastry, K. S. R. (1991). Induction of sperm head abnormalities by incorporated radionuclides: dependence on subcellular distribution, type of radiation, dose rate, and presence of radioprotectors. *Radiat. Res.* **125**: 89-97.

Sasaki, H. (1984). Cell killing and division delay in asynchronous and synchronized HeLa cells irradiated with alpha particles or X-rays. *Radiat. Res.* **99** : 311-323.

Sastry, K. S. (1992). Biological effects of the Auger emitter ^{125}I : a review. Report No. 1 of AAPM Nuclear Medicine Task Group No. 6. *Med. Phys.* **19** (2): 1361-1370.

Sebeela, T. T. (2003). The relative biological effectiveness (RBE) of a 200 MeV clinical proton beam. MSc thesis: North West University, iThemba LABS.

Serengulam, G. V. Goldenberg, D. M., Elsamra, S. E., Griffiths, G. L, Ong, G. L, Brechbiel, M. W, Burton, J, Sgouros, G. Mattes, M. J. (2000). Radionuclides linked to a CD74 antibody as therapeutic agents for B-Cell lymphoma: comparison of Auger electron emitters with β-particle emitters. *Jour. Nuc. Med.* **41** (12) : 2089-2097.

Shard, A. G. and Cowie, B. C. C. (1998). A demonstration of Auger electron emission stimulated by secondary radiation: implications for x-ray standing-wave analysis of surfaces. *J. Phys.: Condens. Matter.* **10** (3): 69-72.

Slabbert, J. P., Langenhoven, J. H. and Smit, B. S. (1999). Synthesis of 4-[^{123}I]iodoantipyrine to study the high-LET characteristics of Auger electrons in mammalian cells. *Journ. Radioanal. Nucl. Chem.* **240** (2): 505-508.

Slabbert, J. P., Theron, T., Serafin, A., Jones, D. T. L., Böhm, L. and Schmitt, G. (1996). Radiosensitivity variations in human tumour cell lines exposed *in vitro* to p(66)/Be neutrons or ^{60}Co γ-rays. *Strahlenther. Onkol.* **172** (10) : 567-572.

Slabbert, J. P., Theron, T., Zölzer, F., Streffer, C. and Böhm, L. (2000). A comparison of the potential therapeutic gain of p(66/Be neutrons and d(14)/Be neutrons. *Int. Journ. Radiat. Oncol. Bio. Phys.* **47** (4): 1059-1065.

Smit, B. S., Slabbert, J. P., Reinecke, S. A. and Böhm, L. (2001). Comparison of cell inactivation by Auger electrons using two reagents 4-[^{123}I]iodoantipyrine and [^{123}I]NaI. *Radiat. Environ. Biophys.* **40**: 47-52.

Stein, R., Govindan, S. V., Mattes, M. J., Chen, S., Reed, L., Newsome, G., McBride, B. J., Griffiths, G. L., Hansen, H. J. and Goldenberg, D. M. (2003). Improved iodine radiolabels for monoclonal antibody therapy. *Cancer Res.* **63** (1): 111-118.

Theron, T., Slabbert, J., Serafin, A. and Böhm, L. (1997). The merits of cell kinetic parameters for the assessment of intrinsic cellular radiosensitivity to photon and high linear energy transfer neutron irradiation. *Int. Journ. Radiat. Oncol. Biol. Phys.* **37** (2): 432-428.

van Leeuwen-Stok A. E., Drager, A. M., Schuurhuis, G. J., Platier, A. W., Teule, G. J. and Huijgens, P. C. (1993). Gallium 67 in the human lymphoma cell line U-715: uptake, cytotoxicity and intracellular localization. *Int. Journ. Radiat Biol.* Vol. **64** (6): 749-759.

van Rooyen, J. (2003). The science of radiation protection. MARST 2003 manual, iThemba LABS.

Volkert, W. A., Goeckeler, W. F., Ehrhardt, G. J. and Ketring A. R. (1991). Therapeutic radionuclides: Production and decay property considerations. *Journ. Nucl. Med.* **32** (1): 174-185.

Walicka, M. A., Adelstein, S. J. and Kassis, A. I. (2001). Chemical modification of 5-[^{125}I]iodo-2′-deoxyuridine toxicity in mammalian cells *in vitro*. *Int. Journ. Radiat. Biol.* **77** (5): 625-630.